RSC Advances

PAPER

View Article Online
View Journal | View Issue

Cite this: *RSC Adv.*, 2025, **15**, 41169

Design, synthesis, *in vitro* cytotoxic activity, and *in silico* studies of symmetrical chlorophenylamino-*s*-triazine derivatives

Em Canh Pham, [ab] Song-Thuong Nguyen,[a] Kim Anh Thi Le,[c] Tuoi Thi Hong Do[a] and Tuyen Ngoc Truong *[a]

Twenty symmetrical chlorophenylamino-*s*-triazine derivatives were designed and synthesized by reflux (RF) and microwave-assisted (MW) methods. The MW method achieved superior yields (88–95%) in less time (15–30 min) compared to RF (78–86%, 12–24 h), particularly for 3-Cl and 3,4-diCl derivatives with piperidine or diethylamine, due to rapid, uniform heating, enhancing nucleophilic substitution and minimizing side reactions. In particular, compounds **2c** (IC_{50} = 4.14 μM for MCF7, 7.87 μM for C26), **3c** (IC_{50} = 4.98 μM for MCF7, 3.05 μM for C26), and **4c** (IC_{50} = 6.85 μM for MCF7, 1.71 μM for C26) exhibited potent cytotoxic activity with **4c** (2,4-diCl, pyrrolidine) surpassing paclitaxel (IC_{50} = 2.30 μM for C26), and **3c** (3,4-diCl, pyrrolidine) rivaling global analogs. Compounds **2f** (IC_{50} = 11.02 μM for MCF7, 4.62 μM for C26) and **3f** (IC_{50} = 5.11 μM for MCF7, 7.10 μM for C26) also showed strong cytotoxicity. QSAR analysis revealed that electron-withdrawing groups (chloro, dichloro) and pyrrolidine enhance C26 potency *via* improved lipophilicity and π–π stacking, outperforming piperazine and morpholine. Pharmacokinetically, **2c**, **3c**, and **4c** matched Bimiralisib's absorption profiles, surpassing Gefitinib, with **4c** showing superior metabolic stability. Compounds **2f** and **3c** emerged as promising multi-targeted kinase inhibitors, with binding affinities (−7.8 to −9.1 kcal mol^{-1}) closely rivaling Gefitinib, Pazopanib, and Bimiralisib for EGFR, VEGFR2, and PI3K, driven by balanced polar and hydrophobic interactions. Therefore, these findings underscore the potential of **2f** and **3c** as multi-targeted kinase inhibitors, warranting further mechanistic studies and structural optimization to enhance MCF7 efficacy and reduce toxicity for clinical advancement.

Received 5th August 2025
Accepted 17th October 2025

DOI: 10.1039/d5ra05705a

rsc.li/rsc-advances

1. Introduction

Heterocyclic compounds, particularly those with five- and six-membered rings, demonstrate a broad spectrum of pharmacological potential.[1–7] Among these, the *s*-triazine core stands out as a critical pharmacophore, driving the development of novel therapeutics with diverse biological effects, including antiviral,[8] antibacterial,[9,10] antifungal,[9,10] anti-inflammatory,[11,12] antimalarial,[13,14] and anticancer activities.[15–28] In addition, the diverse anticancer properties of *s*-triazine derivatives against leukemia, breast cancer, colon cancer, and cervical cancer have attracted considerable research interest.[8] Notably, several *s*-triazine-based drugs with symmetrical structure have emerged as pivotal contributions to global oncology, including Altretamine (anti-ovarian cancer), Tretamine (antineoplastic), Gedatolisib (anti-ovarian cancer, anti-breast cancer, and anti-endometrial cancer), and Bimiralisib (anti-breast cancer).[23] These advancements underscore the *s*-triazine nucleus as a cornerstone in the rational design of targeted cancer therapies (Fig. 1).

A common approach in the synthesis of symmetrical *s*-triazine derivatives is the stepwise substitution of 2,4,6-halogenated *s*-triazines, such as cyanuric chloride, with nucleophiles such as amines, alcohols, or thiols. This method provides precise control over the substitution patterns by exploiting the differential reactivity of chlorine atoms at different temperatures, enabling the sequential introduction of identical substituents to achieve symmetry. In addition, the synthesis from cyanuric chloride stands out due to its operational simplicity, cost-effectiveness, and versatility, especially the possibility of microwave-assisted synthesis to enhance reaction efficiency and yield. Furthermore, this method facilitates the production of high yields of symmetrically substituted *s*-triazines with excellent reproducibility, making it particularly advantageous for both laboratory-scale experiments and industrial applications.[23,29]

[a]*School of Pharmacy, University of Medicine and Pharmacy at Ho Chi Minh City, 700000 Ho Chi Minh City, Vietnam. E-mail: truongtuyen@ump.edu.vn*

[b]*Faculty of Pharmacy, Hong Bang International University, 700000 Ho Chi Minh City, Vietnam*

[c]*UMP Science and Technology Center, University of Medicine and Pharmacy at Ho Chi Minh City, 700000 Ho Chi Minh City, Vietnam*

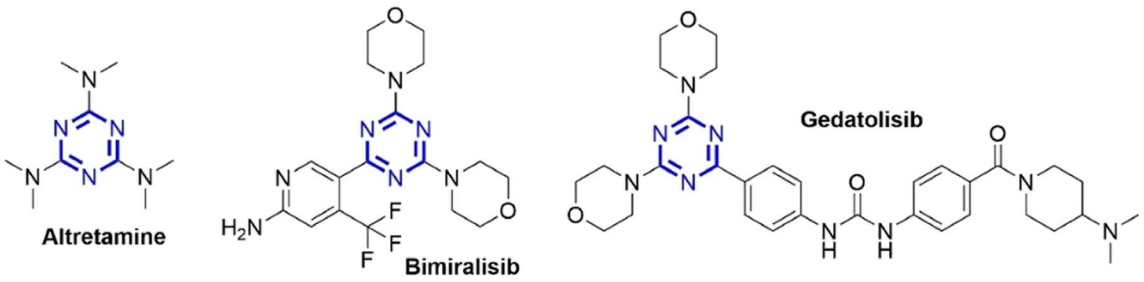

Fig. 1 Anticancer drugs containing *s*-triazine nucleus with symmetrical structure.

1.1 Rational drug design

Symmetrical *s*-triazine derivatives incorporating two saturated cyclic amino groups have emerged as a promising strategy in the development of targeted anticancer therapies, inspired by clinically established *s*-triazine-based drugs such as Altretamine, Tretamine, Gedatolisib (PI3K/mTOR inhibitor), and Bimiralisib (pan-PI3K inhibitor) (Fig. 2). Our published study revealed that symmetrical phenylamino-*s*-triazine derivatives bearing electron-withdrawing groups, such as 4-halogeno (*e.g.*, –Cl) or 4-nitro (–NO_2), on the benzene ring tend to exhibit the most potent cytotoxic activity.[23] For example, 4-chlorophenyl and morpholine substituted triazine analogue not only showed strong activity against C26 (colon carcinoma) with IC_{50} value of 1.21 μM but also demonstrated significantly lower toxicity on normal BAEC cells compared to standard drugs like paclitaxel and doxorubicin,[23] suggesting a better therapeutic index. Therefore, the rational design of new symmetrical chlorophenylamino-*s*-triazine derivatives focuses on replacing the symmetrical triazine ring with saturated cyclic amines, such as piperidine and its derivatives, piperazine and its derivatives, pyrrolidine, or morpholine, to balance lipophilicity, reduce toxicity, and improve cellular uptake. These groups enhance hydrogen bonding and stereospecific interactions with target enzymes or receptors, as seen in Gedatolisib and Bimiralisib, while maintaining synthetic accessibility through nucleophilic substitution on the cyanuric chloride.[23]

In addition, the strategic incorporation of chlorine (Cl) substituents in the rational drug design of symmetrical *s*-triazine derivatives plays a key role in enhancing anticancer potency. Compared to other halogens, chlorine strikes an optimal balance between reactivity and stability, avoiding the excessive instability of fluorine or the bulkiness of bromine, making it ideal for iterative drug optimization. The electron-withdrawing nature of chlorine enhances the electrophilicity of the benzene ring, thereby facilitating interactions with nucleophilic sites on biological targets, such as DNA or proteins involved in cancer cell proliferation. This modification influences the lipophilicity of the compound, improving bioavailability and cellular uptake, which are important factors for effective anticancer agents. Furthermore, several studies have demonstrated that chlorine substitution at specific positions on the benzene ring, particularly *para*- or *meta*-, optimizes cytotoxic activity against various cancer cell lines, including breast and lung carcinomas.[30–32] These findings underscore the strategic importance of chlorine in fine-tuning the physicochemical and pharmacological properties of phenylamino-*s*-triazine derivatives for anticancer applications.

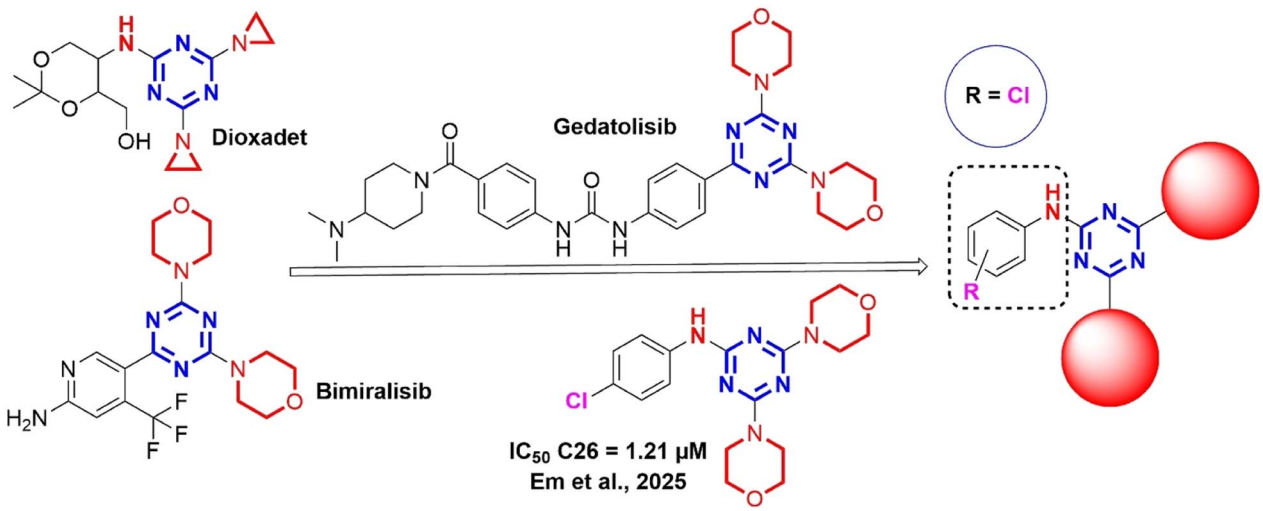

Fig. 2 Rational design of symmetrical chlorophenylamino-*s*-triazine derivatives from anticancer drugs and the potent compound.

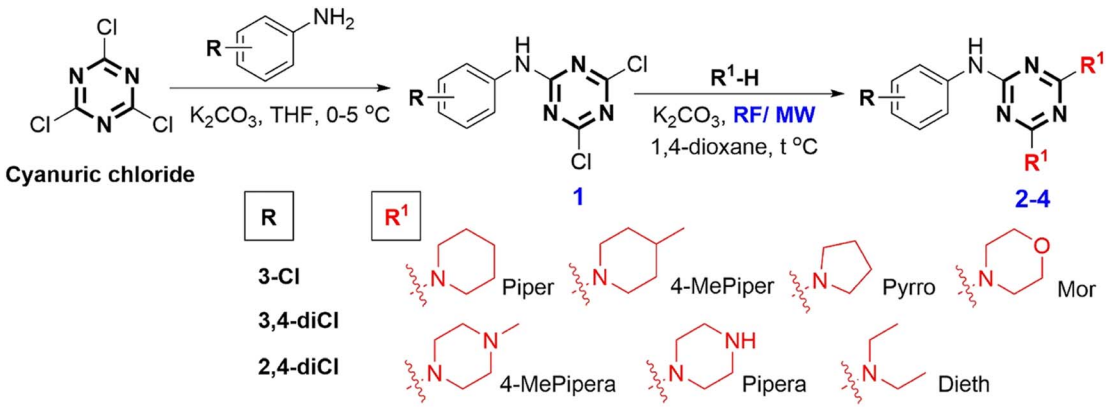

Scheme 1 Synthesis of chlorophenylamino-s-triazine derivatives (MW – microwave irradiation, RF – reflux, THF – tetrahydrofuran).

The strategic design of symmetrical *s*-triazine derivatives, incorporating one chlorophenylamino group and two saturated cyclic amino substituents, represents a robust approach to developing potent anticancer agents, driven by their tailored chemical and pharmacological properties. The chlorophenylamino moiety, characterized by its electron-withdrawing chlorine atom, enhances the lipophilicity of the triazine core and fine-tunes its electronic profile, enabling precise interactions with hydrophobic regions of target proteins, such as receptor tyrosine kinases. The incorporation of saturated cyclic amino groups, such as piperidine, piperazine, or morpholine, optimizes hydrogen-bonding interactions and steric fit, thereby improving binding affinity and target selectivity. Key therapeutic targets for these derivatives include the PI3K/mTOR signaling pathway, as exemplified by Gedatolisib, where cyclic amines enhance aqueous solubility and receptor engagement, demonstrating efficacy in ovarian and breast cancers.[33,34] Additionally, epidermal growth factor receptor (EGFR) and vascular endothelial growth factor receptor 2 (VEGFR2) are promising targets, as the chlorophenylamino group may facilitate specific binding to kinase domains, disrupting oncogenic signaling cascades.[35–37] The balanced lipophilicity and solubility conferred by the combination of chlorophenylamino and cyclic amino groups enhance the derivatives' ability to circumvent multidrug resistance mechanisms, such as efflux pumps. Leveraging structure–activity relationship (SAR) analyses and computational modeling, these *s*-triazine derivatives can be optimized for specific oncogenic pathways, providing a versatile platform for the development of next-generation anticancer therapeutics.

This study aimed to synthesize a series of symmetrical chlorophenylamino-*s*-triazine derivatives incorporating diverse saturated cyclic amino groups and to assess their anticancer efficacy against MCF7 (human breast cancer) and C26 (colon carcinoma) cell lines. The synthesized compounds were evaluated for their cytotoxic potential, with promising candidates selected for further *in silico* molecular docking and ADMET (absorption, distribution, metabolism, excretion, and toxicity) analyses. These investigations seek to elucidate the compounds' interactions with key molecular targets and their pharmacokinetic profiles, providing insights into their therapeutic potential and drug-likeness.

2. Results and discussion

2.1. Chemistry

Mono-substituted *s*-triazine derivatives (yield: 95–97%) were synthesized *via* a nucleophilic substitution reaction between 4-substituted aniline derivatives and cyanuric chloride in tetrahydrofuran (THF) solvent, catalyzed by solid potassium carbonate (K_2CO_3) at a controlled low temperature (0–5 °C). This temperature range ensured selective substitution of the first chlorine atom, enhancing reaction specificity. Subsequently, tri-substituted *s*-triazine derivatives (or chlorophenylamino-*s*-triazine derivatives) were obtained through nucleophilic substitution of the remaining two chlorine atoms on the mono-substituted *s*-triazine derivatives with saturated amines. These reactions were conducted in 1,4-dioxane with solid K_2CO_3 as the base, employing two distinct approaches: conventional reflux (RF) and microwave-assisted (MW) methods (Scheme 1).

The reaction yields of chlorophenylamino-*s*-triazine derivatives using RF and MW methods showed marked differences between different R and R^1 substituents. The MW method consistently outperformed the RF method by 8–13% and achieved higher yields (88–95%) compared to reflux yields (78–86%) across all compounds (**2a–4f**) (Table 1). The microwave method's efficacy stems from its ability to deliver rapid, uniform heating, which accelerates reaction kinetics, enhances nucleophilic substitution on the *s*-triazine core, and minimizes side reactions. This results in improved product purity and yield, particularly for compounds with R groups of 3-Cl (*e.g.*, **2a**, 95%) and 3,4-diCl (*e.g.*, **3a**, 95%) paired with R^1 groups of piperidine (Piper) or diethylamine (Dieth). For group R, compounds with 3-Cl (89–95%), 3,4-diCl (88–95%), and 2,4-diCl (88–93%) substitutions showed similar yield trends. However, regarding R^1 groups, piperidine (Piper) and diethylamine (Dieth) derivatives (*e.g.*, **2a**, **2g**, **3a**, **3g**, **4a**) consistently exhibit higher yields in both methods, likely due to their favorable steric and electronic properties, which enhance nucleophilic substitution on the *s*-

Table 1 Yields and physicochemical parameters of chlorophenylamino-*s*-triazine derivatives (**2a–2g**, **3a–3g** and **4a–4f**)

	R group					Yield (%)	
Entry	R	R^1	Code	Physicochemical parameters[a]		RF	MW
1	3-Cl	Piper	**2a**	MWt: 372.90	MR: 113.28	84	95
				n_{HA}: 3	Log *P*: 5.08		
				n_{HD}: 1	TPSA: 57.18		
				n_{Rot}: 4	Log *S*: −5.43		
2	3-Cl	4-MePiper	**2b**	MWt: 400.95	MR: 122.89	82	91
				n_{HA}: 3	Log *P*: 5.95		
				n_{HD}: 1	TPSA: 57.18		
				n_{Rot}: 4	Log *S*: −6.13		
3	3-Cl	Pyrro	**2c**	MWt: 344.84	MR: 103.66	82	94
				n_{HA}: 3	Log *P*: 4.37		
				n_{HD}: 1	TPSA: 57.18		
				n_{Rot}: 4	Log *S*: −4.84		
4	3-Cl	Mor	**2d**	MWt: 376.84	MR: 105.83	84	92
				n_{HA}: 5	Log *P*: 2.64		
				n_{HD}: 1	TPSA: 75.64		
				n_{Rot}: 4	Log *S*: −3.92		
5	3-Cl	4-MePipera	**2e**	MWt: 402.92	MR: 126.90	79	89
				n_{HA}: 5	Log *P*: 3.01		
				n_{HD}: 1	TPSA: 63.66		
				n_{Rot}: 4	Log *S*: −4.29		
6	3-Cl	Pipera	**2f**	MWt: 374.87	MR: 117.10	82	95
				n_{HA}: 5	Log *P*: 2.08		
				n_{HD}: 3	TPSA: 81.24		
				n_{Rot}: 4	Log *S*: −3.55		
7	3-Cl	Dieth	**2g**	MWt: 348.87	MR: 102.02	85	94
				n_{HA}: 3	Log *P*: 4.86		
				n_{HD}: 1	TPSA: 57.18		
				n_{Rot}: 8	Log *S*: −4.91		
8	3,4-diCl	Piper	**3a**	MWt: 407.34	MR: 118.29	82	95
				n_{HA}: 6	Log *P*: 5.71		
				n_{HD}: 1	TPSA: 57.18		
				n_{Rot}: 4	Log *S*: −6.03		
9	3,4-diCl	4-MePiper	**3b**	MWt: 435.39	MR: 127.90	79	90
				n_{HA}: 3	Log *P*: 6.58		
				n_{HD}: 1	TPSA: 57.18		
				n_{Rot}: 4	Log *S*: −6.73		
10	3,4-diCl	Pyrro	**3c**	MWt: 379.29	MR: 108.67	80	90
				n_{HA}: 3	Log *P*: 4.99		
				n_{HD}: 1	TPSA: 57.18		
				n_{Rot}: 4	Log *S*: −5.43		
11	3,4-diCl	Mor	**3d**	MWt: 411.29	MR: 110.84	78	88
				n_{HA}: 5	Log *P*: 3.27		
				n_{HD}: 1	TPSA: 75.64		
				n_{Rot}: 4	Log *S*: −4.51		
12	3,4-diCl	4-MePipera	**3e**	MWt: 437.37	MR: 131.91	86	94
				n_{HA}: 5	Log *P*: 3.64		
				n_{HD}: 1	TPSA: 63.66		
				n_{Rot}: 4	Log *S*: −4.89		
13	3,4-diCl	Pipera	**3f**	MWt: 409.32	MR: 122.11	83	92
				n_{HA}: 5	Log *P*: 2.71		
				n_{HD}: 3	TPSA: 81.24		
				n_{Rot}: 4	Log *S*: −4.15		
14	3,4-diCl	Dieth	**3g**	MWt: 383.32	MR: 107.03	83	95
				n_{HA}: 3	Log *P*: 5.48		
				n_{HD}: 1	TPSA: 57.18		
				n_{Rot}: 8	Log *S*: −5.50		
15	2,4-diCl	Piper	**4a**	MWt: 407.34	MR: 118.29	82	90
				n_{HA}: 3	Log *P*: 5.71		
				n_{HD}: 1	TPSA: 57.18		
				n_{Rot}: 4	Log *S*: −6.03		
16	2,4-diCl	4-MePiper	**4b**	MWt: 435.39	MR: 127.90	83	92

Table 1 (*Contd.*)

Entry	R group R	R group R^1	Code	Physicochemical parameters[a]		Yield (%) RF	Yield (%) MW
				n_{HA}: 3	Log *P*: 6.58		
				n_{HD}: 1	TPSA: 57.18		
				n_{Rot}: 4	Log *S*: −6.73		
17	2,4-diCl	Pyrro	**4c**	MWt: 379.29	MR: 108.67	81	90
				n_{HA}: 3	Log *P*: 4.99		
				n_{HD}: 1	TPSA: 57.18		
				n_{Rot}: 4	Log *S*: −5.43		
18	2,4-diCl	Mor	**4d**	MWt: 411.29	MR: 110.84	78	88
				n_{HA}: 5	Log *P*: 3.27		
				n_{HD}: 1	TPSA: 75.64		
				n_{Rot}: 4	Log *S*: −4.51		
19	2,4-diCl	4-MePipera	**4e**	MWt: 437.37	MR: 131.91	82	93
				n_{HA}: 5	Log *P*: 3.64		
				n_{HD}: 1	TPSA: 63.66		
				n_{Rot}: 4	Log *S*: −4.89		
20	2,4-diCl	Pipera	**4f**	MWt: 409.32	MR: 122.11	81	90
				n_{HA}: 5	Log *P*: 2.71		
				n_{HD}: 3	TPSA: 81.24		
				n_{Rot}: 4	Log *S*: −4.15		

[a] Calculated using SwissADME, RF – reflux method (/conventional heating), MW – microwave-assisted methods, MWt – molecular weight, n_{HA} – number of hydrogen bond acceptors, n_{HD} – number of hydrogen bond donors, n_{Rot} – number rotatable bonds, TPSA – topological polar surface area (Angstroms squared), MR – molar refractivity, log *P* – log $P_{o/w}$ (XLOGP3), log *S* – log *S* (ESOL).

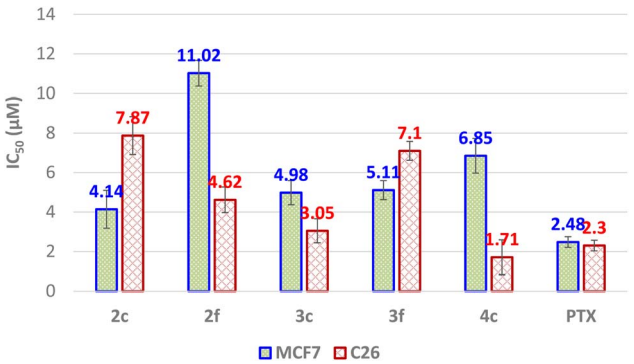

Fig. 3 The IC_{50} values (μM) of potential chlorophenylamino-*s*-triazine derivatives compared to paclitaxel (PTX) (MCF7 – human breast cancer cell line, C26 – colon carcinoma cell line).

triazine core. Conversely, morpholine (Mor) derivatives (*e.g.*, **2d**, **3d**, **4d**) show the lowest yields (78–88%), potentially due to reduced nucleophilicity (Table 1). These findings align closely with those reported by Al-Zaydi *et al.* (2017), who utilized 4-carboxyaniline as the starting material for tri-substitution reactions with saturated cyclic amines (piperidine and morpholine) in a 1 : 1 mixture of 1,4-dioxane and water, using sodium carbonate (Na_2CO_3) as the base. Their study achieved yields of 74.5–85.8% over 8–10 h under RF conditions, and 88–93.1% in 10 min using MW irradiation at 400 W.[38] In particular, our published research highlights the superior yields of the MW method in synthesizing tri-substituted *s*-triazine derivatives (R = 4-Cl, 4-F, 4-OCH_3, 4-CH_3, 4-NO_2; R^1 = Piper, Mor), achieving excellent yields (91–98%) and rapid reaction times (15–30 min). In contrast, the RF method required significantly longer reaction times (12–24 h) and lower yields (80–88%).[23] Therefore, these findings underscore the advantages of the MW method ("green" approach) in terms of efficiency, speed, and environmental protection, offering a scalable, efficient, and environmentally friendly approach for producing potential anticancer agents.

The chemical structures of chlorophenylamino-*s*-triazine derivatives were suitably elucidated by ^{1}H NMR, ^{13}C NMR, and MS spectroscopy. The ^{1}H and ^{13}C NMR spectra of chlorophenylamino-*s*-triazine derivatives (**2a–2g**, **3a–3g**, **4a–4f**) provide critical insights into their structural characteristics, highlighting the influence of varying R and R^1 substituents on the *s*-triazine core. In the ^{1}H NMR spectra, the –NH– proton, linking the chlorophenyl moiety to the triazine ring, consistently appears as a singlet in the range of 8.05–10.76 ppm, with compounds bearing 3,4-dichlorophenyl (9.03–9.41 ppm) and 3-chlorophenyl (9.13–10.76 ppm) groups showing slight downfield shifts compared to 2,4-dichlorophenyl derivatives (8.00–8.31 ppm). This variation reflected the electron-withdrawing effects of additional chlorine atoms, which modulate the electron density around the –NH– group. Aromatic protons (H_{Ar}) on the chlorophenyl ring exhibited characteristic splitting patterns, with 3-chlorophenyl derivatives showing a triplet and doublets at δ 6.90–8.16 ppm, while 3,4-dichlorophenyl and 2,4-dichlorophenyl compounds display simplified patterns due to increased substitution, as seen in the doublet at δ 8.35 ppm for **3a**. The R^1 cyclic amino groups significantly influence aliphatic signals; for instance, pyrrolidine (**2a**, **3a**, **4a**) showed distinct –

Table 2 Anticancer activity of chlorophenylamino-*s*-triazine derivatives (IC_{50}, μM)[a]

Entry	Code	Cancer cell line	
		MCF7 (IC_{50}, μM)	C26 (IC_{50}, μM)
1	**2a**	28.20 ± 1.68	23.05 ± 1.25
2	**2b**	24.37 ± 0.66	20.53 ± 0.65
3	**2c**	**4.14 ± 1.06**	**7.87 ± 0.96**
4	**2d**	38.02 ± 3.85	21.54 ± 0.81
5	**2e**	19.64 ± 1.37	47.53 ± 1.03
6	**2f**	**11.02 ± 0.68**	**4.62 ± 0.65**
7	**2g**	36.67 ± 1.85	58.17 ± 2.19
8	**3a**	36.02 ± 2.26	29.14 ± 2.63
9	**3b**	36.33 ± 0.76	21.77 ± 1.10
10	**3c**	**4.98 ± 0.58**	**3.05 ± 0.61**
11	**3d**	28.36 ± 1.88	30.71 ± 4.25
12	**3e**	37.38 ± 3.47	24.25 ± 1.34
13	**3f**	**5.11 ± 0.31**	**7.10 ± 0.48**
14	**3g**	55.62 ± 5.30	37.58 ± 0.88
15	**4a**	40.85 ± 0.41	46.55 ± 1.42
16	**4b**	25.09 ± 1.39	48.55 ± 1.30
17	**4c**	**6.85 ± 0.34**	**1.71 ± 0.88***
18	**4d**	43.03 ± 0.96	39.15 ± 2.96
19	**4e**	10.05 ± 0.36	16.38 ± 0.63
20	**4f**	17.04 ± 1.00	17.15 ± 0.83
21	**PTX**	2.48 ± 0.51	2.30 ± 0.27

[a] All data are presented as mean ± standard deviation (SD), PTX – paclitaxel, MCF7 – human breast cancer cell line, C26 – colon carcinoma cell line, the values in bold highlight the best compounds with the best IC_{50} values compared to the positive control, * – statistically significant ($p < 0.05$) compared to reference drug PTX.

CH_2– triplets at δ 3.46–3.49 ppm, whereas morpholine (**2d**, **3d**, **4d**), piperazine (**2e**, **3e**, **4e**) and its derivatives (**2b**, **3b**, **4b**) exhibited additional oxygen/nitrogen-adjacent –CH_2– signals at δ 3.59–3.70 ppm, reflecting its heterocyclic nature. Piperidine derivatives (**2f**, **3f**, **4f**) display broader –CH_2– signals at δ 1.47–3.70 ppm, indicating greater conformational flexibility. In the ^{13}C NMR spectra, the triazine ring carbons resonated at δ 163.1–165.0 ppm, with minor shifts attributed to the electronic effects of R^1 substituents. For example, morpholine derivatives (**2d**, **3d**, **4d**) showed a characteristic carbon signal at δ 65.9–66.3 ppm for oxygen-linked –CH_2–, absent in piperidine or pyrrolidine analogs. The chlorophenyl carbons appear at δ 117.3–142.6 ppm, with 3,4-dichlorophenyl compounds (*e.g.*, **3a**) showing a downfield shift (δ 141.0 ppm) compared to 2,4-dichlorophenyl analogs (*e.g.*, **4a**, δ 135.4 ppm), reflecting differences in chlorine positioning. Aliphatic carbons of R^1 groups, such as pyrrolidine (δ 24.3–24.8 ppm) and piperidine (δ 24.3–25.8 ppm), are consistent across series, while methyl-substituted piperazines (**2b**, **3b**, **4b**) introduced additional signals at δ 42.5–54.5 ppm. Moreover, the mass spectrometry analysis revealed the molecular ion peak (*M*, *m*/*z*) for compounds **2–4**, corroborating their proposed structures. Notably, all chlorophenylamino-*s*-triazine derivatives exhibited physicochemical properties, including molecular weights (MWt < 500), consistent with Lipinski's rule of five (Table 1). These characteristics suggest their potential as promising candidates for further drug development.

2.2. *In vitro* anticancer activity

The cytotoxic activities of a series of compounds (**2a–2g**, **3a–3g**, **4a–4f**) were evaluated against MCF7 (human breast cancer) and C26 (murine colon carcinoma) cell lines, with IC_{50} values indicating the concentration required to inhibit 50% of cell growth (Table 2). These results were benchmarked against paclitaxel (PTX), a standard chemotherapeutic agent. Among the series of **2**, compounds **2c** and **2f** exhibited the highest cytotoxic activities. Compound **2c** demonstrated IC_{50} values of 4.14 ± 1.06 μM (MCF7) and 7.87 ± 0.96 μM (C26), while **2f** showed 11.02 ± 0.68 μM (MCF7) and 4.62 ± 0.65 μM (C26). Notably, **2f**'s activity against C26 approaches that of PTX, suggesting strong potential against colon carcinoma. In contrast, compounds **2a** (28.20 ± 1.68 μM for MCF7, 23.05 ± 1.25 μM for C26), **2b** (24.37 ± 0.66 μM for MCF7, 20.53 ± 0.65 μM for C26), **2d** (38.02 ± 3.85 μM for MCF7, 21.54 ± 0.81 μM for C26), **2e** (19.64 ± 1.37 μM for MCF7, 47.53 ± 1.03 μM for C26), and **2g** (36.67 ± 1.85 μM for MCF7, 58.17 ± 2.19 μM for C26) displayed significantly higher IC_{50} values, indicating weaker cytotoxicity. The superior activity of **2c** and **2f** likely stems from specific structural features enhancing their interaction with cellular targets, such as tubulin, similar to PTX's microtubule-stabilizing mechanism.

In the series **3** compounds, **3c** and **3f** stood out as the most potent. Compound **3c** exhibited IC_{50} values of 4.98 ± 0.58 μM (MCF7) and 3.05 ± 0.61 μM (C26), with its C26 activity closely rivaling PTX. Compound **3f** showed IC_{50} values of 5.11 ± 0.31 μM (MCF7) and 7.10 ± 0.48 μM (C26), also indicating strong cytotoxicity. Other compounds, including **3a** (36.02 ± 2.26 μM for MCF7, 29.14 ± 2.63 μM for C26), **3b** (36.33 ± 0.76 μM for MCF7, 21.77 ± 1.10 μM for C26), **3d** (28.36 ± 1.88 μM for MCF7, 30.71 ± 4.25 μM for C26), **3e** (37.38 ± 3.47 μM for MCF7, 24.25 ± 1.34 μM for C26), and **3g** (55.62 ± 5.30 μM for MCF7, 37.58 ± 0.88 μM for C26), showed moderate to low activity, with IC_{50} values 10- to 20-fold higher than PTX. The potency of **3c** and **3f** suggests favorable molecular interactions, possibly involving enhanced binding affinity to apoptotic or mitotic pathways.

Series **4** compounds revealed **4c** and **4e** as the most effective. Compound **4c** was particularly notable, with IC_{50} values of 6.85 ± 0.34 μM (MCF7) and 1.71 ± 0.88 μM (C26), the latter surpassing PTX's potency against C26. Compound **4e** showed IC_{50} values of 10.05 ± 0.36 μM (MCF7) and 16.38 ± 0.63 μM (C26), indicating moderate activity. Other compounds, such as **4a** (40.85 ± 0.41 μM for MCF7, 46.55 ± 1.42 μM for C26), **4b** (25.09 ± 1.39 μM for MCF7, 48.55 ± 1.30 μM for C26), **4d** (43.03 ± 0.96 μM for MCF7, 39.15 ± 2.96 μM for C26), and **4f** (17.04 ± 1.00 μM for MCF7, 17.15 ± 0.83 μM for C26), exhibited lower potency. The exceptional activity of **4c**, particularly against C26, suggests a highly optimized structure for targeting colon carcinoma cells, potentially through mechanisms akin to PTX's disruption of microtubule dynamics.

PTX remains the gold standard with IC_{50} values of 2.48 ± 0.51 μM (MCF7) and 2.30 ± 0.27 μM (C26). Among the tested compounds, **4c** stands out as the only compound surpassing

Table 3 ADMET profile of the active compounds and reference drugs[a]

Parameter	2c		2f		3c		3f		4c		Ged		Bim	
Druglikeness														
Lipinski	Yes		Yes		Yes		Yes		Yes		No		Yes	
Ghose	Yes		No		Yes		No		Yes		No		Yes	
Veber	Yes		Yes		Yes		Yes		Yes		Yes		Yes	
Egan	Yes		Yes		Yes		Yes		Yes		Yes		Yes	
Muegge	Yes		Yes		Yes		Yes		Yes		No		Yes	
Pfizer	No		Yes		No		Yes		No		Yes		Yes	
Bioavailability score	0.55		0.55		0.55		0.55		0.55		0.17		0.55	
SAscore	<6	E	<6	E	<6	E	<6	E	<6	E	<6	E	<6	E
Absorption														
Caco-2 permeability	−4.883	E	−5.283	P	−5.105	E	−5.569	P	−4.942	E	−5.322	P	−4.546	E
MDCK permeability	0	E	0	E	0	E	0	E	0	E	0.0	E	0	E
PAMPA	−−−	E	−−	E	−−−	E	−	M	−−−	E	−−−	E	−−−	E
Pgp-inhibitor	+++	P	−−−	E	+++	P	−−−	E	+++	P	+++	P	+++	P
Pgp-substrate	−−−	E	+++	P	−−−	E	+++	P	−−−	E	+++	P	−−−	E
HIA	−−−	E	−−−	E	−−−	E	−−−	E	−−−	E	−−−	E	−−−	E
$F_{20\%}$	−−−	E	−−−	E	−−−	E	−−−	E	−−−	E	−−−	E	−−−	E
$F_{30\%}$	−−−	E	−−−	E	−−−	E	−−−	E	−−−	E	−−−	E	−−−	E
$F_{50\%}$	+++	P	++	P	+++	P	+++	P	−−	E	+++	P	−−−	E
Distribution														
PPB (%)	99.60	P	78.00	E	99.60	P	79.50	E	99.50	P	76.5	E	94.20	P
VDss (L kg^{-1})	3.546	E	6.224	E	4.144	E	5.6750	E	3.3880	E	2.6600	E	2.576	E
BBB penetration	−−−	E	−	M	−	M	++	P	+	M	−−−	E	++	P
Fu (%)	0.30	P	20.50	E	0.30	P	16.40	E	0.40	P	18.0	E	6.30	E
OATP1B1 inhibitor	+++	P	+++	P	+++	P	+++	P	+++	P	+++	P	++	P
OATP1B3 inhibitor	+++	P	+++	P	+++	P	+++	P	+++	P	+++	P	+++	P
BCRP inhibitor	+++	P	−−−	P	++	P	−−−	P	+	M	−−−	P	−−−	P
MRP1 inhibitor	++	P	++	P	−	M	−	M	+++	P	−	M	+++	P
BSEP inhibitor	+++	P	+	P	+++	P	+++	P	+++	P	+++	P	−	P
Metabolism														
CYP1A2 inhibitor	+++		+++		+++		+++		+++		+++		+++	
CYP1A2 substrate	+++		+++		+++		+++		+++		−−−		−−−	
CYP2C19 inhibitor	−−		−−−		++		−		−		−−−		−−−	
CYP2C19 substrate	−−−		+++		−−		+++		+++		+++		+++	
CYP2C9 inhibitor	+++		+		+++		+++		+++		−−−		++	
CYP2C9 substrate	−−−		−−−		−−−		−−−		−−−		−−−		+++	
CYP2D6 inhibitor	++		−−−		+++		−−		−		−−−		−−−	
CYP2D6 substrate	−−−		−−−		−−−		−−−		−−−		−−−		−−−	
CYP3A4 inhibitor	−−		+++		+		+++		−		−−−		−−−	
CYP3A4 substrate	−−−		+++		+++		+++		+++		++		−−−	
CYP2B6 inhibitor	+++		−−−		+++		−−−		+++		+++		−−−	
CYP2B6 substrate	−−−		−−−		−−−		−−−		−−−		−−−		−−−	
CYP2C8 inhibitor	+++		++		+++		−−		−−−		−−		−−−	
HLM stability	−	M	−−	P	+	M	−−−	P	++	E	−−−	P	−−−	P
Excretion														
CL_{plasma} (mL min^{-1} kg^{-1})	4.52	E	4.222	E	4.72	E	4.293	E	5.437	M	5.329	M	5.41	M
$T_{1/2}$	0.609		0.47		0.82		0.65		0.682		0.297		0.926	
Toxicity														
hERG blockers	0.663	M	0.953	P	0.728	P	0.965	P	0.639	M	0.949	P	0.272	E
hERG blockers (10 μm)	0.846	P	0.868	P	0.872	P	0.890	P	0.856	P	0.337	M	0.359	M
DILI	0.772	P	0.990	P	0.845	P	0.994	P	0.832	P	0.998	P	0.985	P
AMES toxicity	0.167	E	0.264	E	0.145	E	0.234	E	0.125	E	0.545	M	0.503	M
Rat oral acute toxicity	0.202	E	0.720	P	0.237	E	0.756	P	0.263	E	0.289	E	0.428	M
FDAMDD	0.521	M	0.330	P	0.541	M	0.350	M	0.473	M	0.457	M	0.212	E
Skin sensitization	0.420	M	0.922	P	0.462	M	0.932	P	0.275	E	0.635	M	0.286	E
Carcinogenicity	0.652	M	0.149	E	0.670	M	0.162	E	0.709	P	0.947	P	0.955	P
Eye corrosion	0	E	0.088	E	0.001	E	0.124	E	0.001	E	0.0	E	0	E
Eye irritation	0.57	M	0.743	P	0.416	M	0.608	M	0.343	M	0.0	E	0.423	M

Table 3 (*Contd.*)

Parameter	2c		2f		3c		3f		4c		Ged		Bim	
Respiratory toxicity	0.484	M	0.998	P	0.463	M	0.998	P	0.487	M	0.791	P	0.733	P
Human hepatotoxicity	0.782	P	0.987	P	0.766	P	0.986	P	0.805	P	0.986	P	0.967	P
Drug-induced nephrotoxicity	0.738	P	0.999	P	0.815	P	1	P	0.769	P	0.997	P	0.982	P
Drug-induced neurotoxicity	0.774	P	0.993	P	0.844	P	0.995	P	0.856	P	0.991	P	0.994	P
Ototoxicity	0.395	M	0.842	P	0.479	M	0.883	P	0.507	M	0.864	P	0.85	P
Hematotoxicity	0.238	E	0.546	M	0.319	M	0.642	M	0.305	M	0.475	M	0.323	M
Genotoxicity	0.925	P	0.999	P	0.828	P	0.999	P	0.741	P	1.0	P	1	P
RPMI-8226 immunotoxicity	0.073	E	0.070	E	0.080	E	0.076	E	0.066	E	0.624	M	0.36	M
A549 cytotoxicity	0.617	M	0.639	M	0.722	P	0.738	P	0.67	M	0.051	E	0.074	E
Hek293 cytotoxicity	0.874	P	0.391	M	0.9	P	0.457	M	0.864	P	0.749	P	0.424	M
BCF	1.490		0.789		1.817		1.266		1.889		0.755		0.632	
IGC50	3.841		3.287		4.119		3.696		4.005		3.379		3.241	
LC50DM	5.113		4.651		5.232		4.810		5.413		5.31		4.997	
LC50FM	4.722		4.030		5.012		4.473		5.046		4.206		3.899	

[a] Ged – Gedatolisib, Bim – Bimiralisib, Caco-2 permeability (optimal: higher than −5.15 log unit), MDCK permeability (low permeability: $<2 \times 10^{-6}$ cm s^{-1}, medium permeability: 2–20 $\times 10^{-6}$ cm s^{-1}, high passive permeability: $>20 \times 10^{-6}$ cm s^{-1}), PAMPA – the experimental data for P_{eff} was logarithmically transformed ($\log P_{eff} < 2$: low-permeability, $\log P_{eff} > 2.5$: high-permeability), Pgp – P-glycoprotein, HIA – human intestinal absorption (−: ≥30%, +: < 30%), *F*: bioavailability (+: < percent value, −: ≥ percent value), PPB: plasma protein binding (optimal: < 90%), VD: volume distribution (optimal: 0.04–20 L kg^{-1}), BBB: blood–brain barrier penetration, Fu: the fraction unbound in plasms (low: <5%, middle: 5–20%, high: > 20%), CL : Clearance (low: < 5 $mLmin^{-1}kg$, moderate: 5–15 mL min^{-1} kg^{-1}, high: > 15 mL min^{-1} kg^{-1}), $T_{1/2}$ (ultra-short half-life drugs: 0.5 – < 1 h; short half-life drugs: 1–4 h; intermediate short half-life drugs: 4–8 h; long half-life drugs: >8 h), hERG blockers ($IC_{50} \leq 10$ μM or ≥ 50% inhibition at 10 μM were classified as hERG +, $IC_{50} > 10$ μM or <50% inhibition at 10 μM were classified as hERG −−), DILI: drug-induced liver injury, rat oral acute toxicity (0: low-toxicity > 500 mg kg^{-1}, 1: high-toxicity < 500 mg kg^{-1}), FDAMDD – maximum recommended daily dose, BCF – bioconcentration factors, IGC50 – tetrahymena pyriformis 50 percent growth inhibition Concentration, LC50FM – 96 h fathead minnow 50 percent lethal concentration, LC50DM – 48 h daphnia magna 50 percent lethal concentration. The output value is the probability of being inhibitor/substrate/active/positive/high-toxicity/sensitizer/carcinogens/corrosives/irritants (category 1) or non-inhibitor/non-substrate/inactive/negative/low-toxicity/non-sensitizer/non-carcinogens/noncorrosives/nonirritants (category 0). For the classification endpoints, the prediction probability values are transformed into six symbols: 0–0.1(−−−), 0.1–0.3(−−), 0.3–0.5(−), 0.5–0.7(+), 0.7–0.9(++), and 0.9–1.0(+++). Additionally, the corresponding relationships of the three labels are as follows: E − excellent, M – medium, P – poor.

PTX's potency against C26, while **3c** and **2f** closely approach it. Against MCF7, compounds **2c**, **3c**, and **3f** showed promising activity but remain less potent than PTX. The weaker performance of most compounds, particularly **2g**, **3g**, **4a**, and **4d**, underscores the challenge of achieving PTX's broad-spectrum efficacy. Structural modifications in **2c**, **3c**, **3f**, and **4c** likely enhance their cytotoxic potential, possibly by improving solubility, cellular uptake, or target specificity, but further studies are needed to elucidate their mechanisms and optimize their activity to match or exceed PTX.

In conclusion, compounds **2c** (3-Cl, pyrrrolidine), **2f** (3-Cl, piperazine), **3c** (3,4-diCl, pyrrrolidine), **3f** (3,4-diCl, piperazine), and **4c** (2,4-diCl, pyrrrolidine) exhibited significant cytotoxic potential, with **4c** showing superior activity against C26 compared to PTX (Fig. 3). The results also suggested that the R^1 substituents such as pyrrolidine and piperazine in these derivatives may be responsible for their potential cytotoxic activity. These compounds warrant further investigation for structural optimization and mechanism studies to enhance their efficacy, especially against MCF7 cells, where PTX still retains a clear advantage.

2.3. Structure–activity relationships (SAR)

The cytotoxic activities of five *s*-triazine derivatives (**2c**, **2f**, **3c**, **3f**, and **4c**) against MCF7 and C26 cell lines were compared with structurally analogous *s*-triazine derivatives reported globally to elucidate their anticancer potential and establish quantitative structure–activity relationships (QSAR). Compound **2c**, with 3-chlorophenyl and pyrrolidine (IC_{50}: 4.14 μM for MCF7, 7.87 μM for C26) outperformed 4-bromophenylamino-*s*-triazine derivatives with pyrazolyl and morpholino groups (IC_{50}: 4.53 μM for MCF7),[39] likely due to the pyrrolidine groups enhancing molecular flexibility and hydrophobic interactions with cellular targets like tubulin. Compound **2f**, with piperazine substitutions (IC_{50}: 11.02 for MCF7, 4.62 μM for C26) showed superior C26 activity compared to 4,6-dimorpholino-*s*-triazine with a 4-acylphenylamino group (IC_{50}: 8.71 μM for SW620),[20] suggesting that piperazine enhances colon cancer specificity, possibly *via* increased hydrogen bonding. Compound **3c**, with 3,4-dichlorophenyl and pyrrolidine (IC_{50}: 4.98 μM for MCF7, 3.05 μM for C26) rivaled 4-bromo/4-chlorophenylamino-*s*-triazines with indol-3-ylpyrazolyl groups (IC_{50}: 2–4 μM for MCF7),[18] with its dichlorophenyl group likely strengthening π–π stacking and electron-withdrawing effects, enhancing C26 potency. Compound **3f**, with piperazine groups (IC_{50}: 5.11 μM for MCF7, 7.10 μM for C26), is less effective against C26 than **3c**, aligning with findings that pyrrolidine outperforms piperazine in colon cancer models. Compound **4c**, with 2,4-dichlorophenyl and pyrrolidine (IC_{50}: 6.85 μM for MCF7, 1.71 μM for C26), surpassed the 4-bromophenylamino-*s*-triazine (IC_{50} : 0.50 μM for HCT-116),[39] with the ortho-chlorine likely optimizing steric and electronic interactions for exceptional C26 activity. QSAR

Table 4 *In silico* molecular docking results of potent chlorophenylamino-*s*-triazine derivatives and reference drugs[a]

		EGFR			VEGFR2			PI3K		
Entry	Compound	BA	Bond type (Å)	AA	BA	Bond type (Å)	AA	BA	Bond type (Å)	AA
1	**2c**	−7.4	1 π-sulfur (3.52), 11 hydrophobic (3.66–5.48)	LEU844, MET790, LEU718, CYS797, LYS745, LEU788, ALA743, VAL726	−8.8	13 hydrophobic (3.72–5.50)	VAL846, VAL914, LEU838, ALA864, LEU1033, LEU887, VAL897, PHE1045, LYS866	−8.8	1 HB (3.58), 10 hydrophobic (3.60–5.50)	ASP964, ILE963, TYR867, ILE879, ALA885, ILE881, VAL882, MET953, PHE961
2	**2f**	−7.8	2 HB (2.27, 3.48), 4 hydrophobic (3.56–4.84)	GLU762, THR854, LEU718, LEU844, ALA743	−8.9	1 HB (2.10), 8 hydrophobic (4.13–5.45)	CYS917, LYS866, VAL912, VAL914, VAL846, CYS1043, VAL897	−9.0	1 HB (2.78), 8 hydrophobic (3.68–5.16)	ASP836, ILE963, TYR867, ALA885, ILE881, VAL882, MET953
3	**3c**	−7.6	8 Hydrophobic (3.64–5.35)	LEU718, LYS745, LEU788, MET790, LEU844, ALA743	−9.1	2 HB (3.53, 3.38), 16 hydrophobic (3.49–5.48)	LEU838, VAL846, VAL914, ARG840, LYS866, VAL912, LEU887, VAL897, LEU1033, ALA864	−8.7	8 Hydrophobic (3.79–5.38)	ILE963, ILE879, VAL882, MET953, TYR867, ILE831
4	**3f**	−7.8	1 HB (2.85), 6 hydrophobic (3.66–5.17)	GLU762, LEU718, LEU792, LEU844, ALA743	−8.9	1 HB (3.54), 11 hydrophobic (3.89–5.47)	ASP1044, VAL846, VAL914, LEU887, VAL897, VAL912, PHE1045, CYS1043	−8.8	2 HB (2.96, 2.91), 1 electrostatic (4.19), 1 DHB (3.06), 5 hydrophobic (3.59–4.34)	SER806, ASP841, ASP964, LYS807, ILE968
5	**4c**	−7.7	12 Hydrophobic (3.63–5.48)	LEU718, ALA743, LYS745, LEU788, MET790, CYS797, LEU844, MET793, VAL726	−8.6	2 HB (3.60, 3.33), 15 hydrophobic (3.76–5.43)	LEU838, VAL846, VAL914, ARG840, LEU1033, LYS866, LEU887, PHE1045, VAL897, CYS1043	−8.6	7 Hydrophobic (3.65–5.44)	ILE963, ILE879, VAL882, MET953, TYR867, ILE831
6	Gefitinib	−7.3	1 HB (3.54), 1 π-sulfur (3.56), 8 hydrophobic (3.83–5.48)	ASP855, MET790, LEU718, VAL726, ALA743, LEU844, LYS745	—	—	—	—	—	—
7	Pazopanib	—	—	—	−10.0	1 HB (3.69), 9 hydrophobic (3.64–5.43)	GLU883, LEU838, LEU1033, LYS866, VAL914, ALA864, VAL846, VAL897, CYS1043	—	—	—
8	Bimiralisib	—	—	—	—	—	—	−9.1	2 HB (2.05, 3.28), 1 electrostatic (4.15), 11 hydrophobic (3.59–5.47)	VAL882, ASP836, ASP964, ILE879, ILE963, ILE881, ALA885, MET953, PRO810, ILE831, LYS833

[a] BA – binding affinity (kcal mol^{-1}), bond type (distance/bond length – Å), AA – amino acid, HB–hydrogen bond (conventional/strong hydrogen bond), CHB – carbon–hydrogen bond, DHB – π-donor hydrogen bond, EGFR – epidermal growth factor receptor, VEGFR2 – vascular endothelial growth factor receptor 2, PI3K – phosphoinositide 3-kinase.

analysis reveals that electron-withdrawing groups (*e.g.*, chloro, dichloro) on the phenyl ring enhance cytotoxicity, particularly against C26, as seen in 4-halogeno and 4-nitro substituted triazines.[23] Pyrrolidine substitutions consistently improve potency over piperazine, likely due to increased lipophilicity and reduced steric hindrance, while dichlorophenyl groups amplify activity compared to monochlorophenyl, correlating with higher electron-withdrawing capacity. Compared to sulfaguanidine-triazines (IC_{50}: 14.8–33.2 μM for MCF7),[21] these compounds exhibited superior potency, though less toxic than doxorubicin (IC_{50}: 0.42 μM),[18] suggesting a favorable therapeutic index.

Compared more specifically with our published research, in examining the cytotoxic activities of five chlorophenylamino-*s*-triazine derivatives (**2c**, **2f**, **3c**, **3f**, and **4c**) against MCF7 and C26 cell lines, these compounds generally exhibited superior potency compared to the three phenylamino-*s*-triazine analogs (**P-2e** (4-nitrophenyl and piperidine substituted triazine), **P-3a** (4-chlorophenyl and morpholine substituted triazine), and **P-3e** (4-nitrophenyl and morpholine substituted triazine)), as evidenced by their lower IC_{50} values. For the MCF7 line, the potent chlorophenyl series displayed IC_{50} ranges from 4.14 ± 1.06 μM (**2c**) to 11.02 ± 0.68 μM (**2f**), markedly outperforming the phenyl series, which spans 13.74 ± 1.96 μM (**P-3e**) to 42.40 ± 4.48 μM

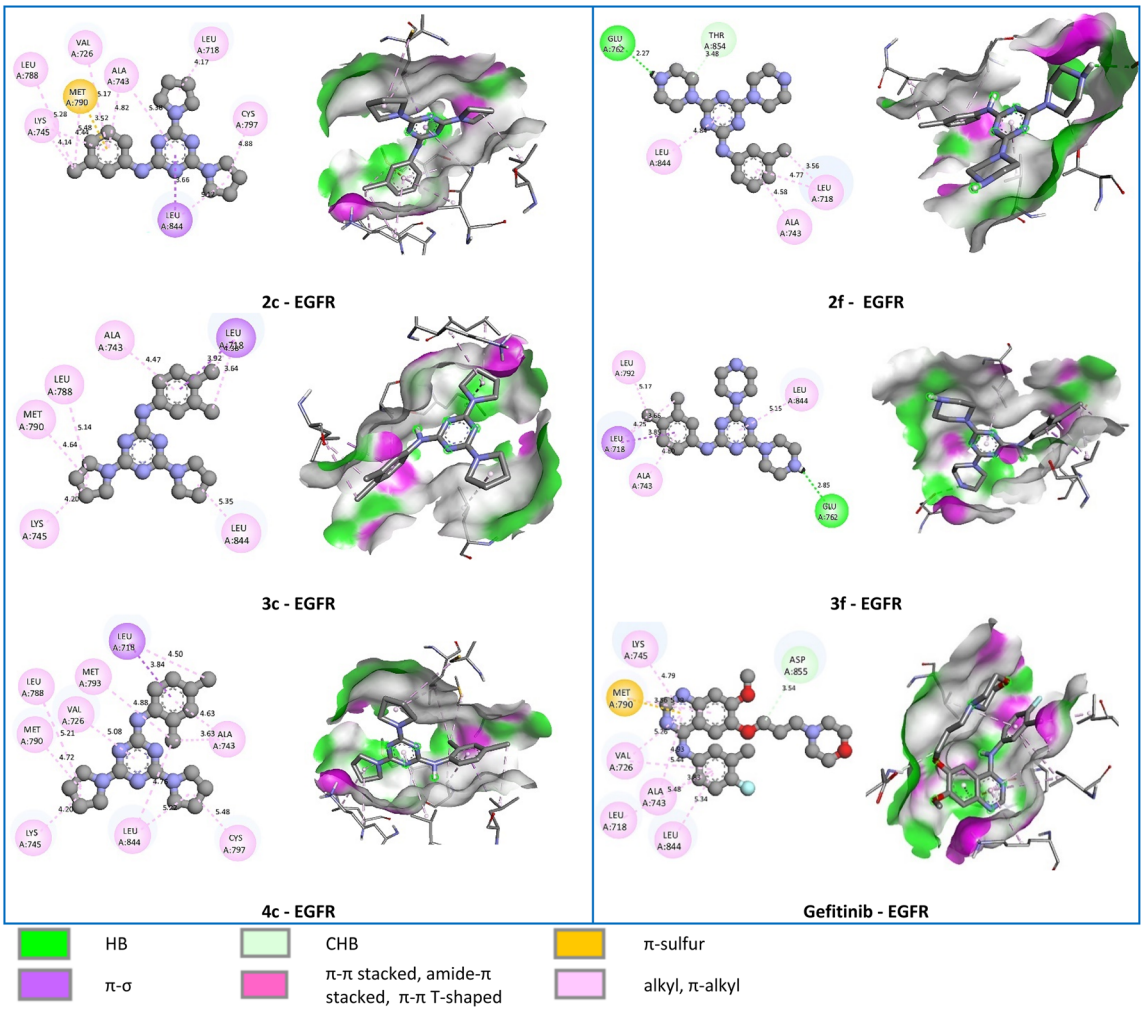

Fig. 4 2D and 3D representation of the interaction of potent chlorophenylamino-*s*-triazine derivatives and reference drug Gefitinib with epidermal growth factor receptor (EGFR) target.

(**P-3a**), suggesting that chlorine substitution on the phenyl ring enhances selectivity and efficacy against this estrogen receptor-positive breast cancer model, potentially through improved lipophilicity or π–π stacking interactions with cellular targets. In contrast, on the C26 line, the chlorophenyl compounds yield IC_{50} values from 1.71 ± 0.88 μM (**4c**) to 7.87 ± 0.96 μM (**2c**), overlapping with but not consistently surpassing the phenyl analogs (1.21 ± 0.47 μM for **P-3a** to 14.66 ± 1.70 μM for **P-3e**), indicating a more variable response where certain chlorine positions, such as the 2,4-dichloro motif in **4c**, confer exceptional activity possibly *via* steric hindrance or altered electron withdrawal affecting membrane permeability.

In summary, QSAR analysis of chlorophenylamino-*s*-triazine derivatives underscores the pivotal role of strategic substitutions in modulating cytotoxic efficacy against MCF7 breast cancer and C26 colon cancer cell lines. Electron-withdrawing chloro groups on the phenyl ring, particularly in di-substituted configurations such as 3,4-dichloro (**3c**) and 2,4-dichloro (**4c**), significantly enhance potency against C26. Moreover, pyrrolidine moieties consistently outperform piperazine counterparts and tend to favor lower IC_{50} on MCF7 compared to piperazine, as seen in the superior activity of **2c** and **3c** over **2f** and **3f**, attributable to enhanced molecular flexibility, reduced steric hindrance, and stronger hydrophobic engagements, while piperazine confers selective hydrogen-bonding advantages in colon cancer models. While less potent than doxorubicin, their favorable therapeutic indices position compounds like **4c** and **3c** as promising scaffolds for lead optimization, warranting deeper mechanistic investigations into tubulin-binding dynamics and *in vivo* pharmacokinetics to advance anticancer therapeutics.

2.4. *In silico* ADMET profile

The *in silico* ADMET profile of the five potent compounds and reference drugs Gedatolisib (Ged) and Bimiralisib (Bim) is shown in Table 3.

2.4.1. Druglikeness. The druglikeness of five *s*-triazine derivatives (**2c**, **2f**, **3c**, **3f**, and **4c**) was evaluated against reference drugs Gedatolisib (Ged) and Bimiralisib (Bim) using established physicochemical and pharmacokinetic filters,

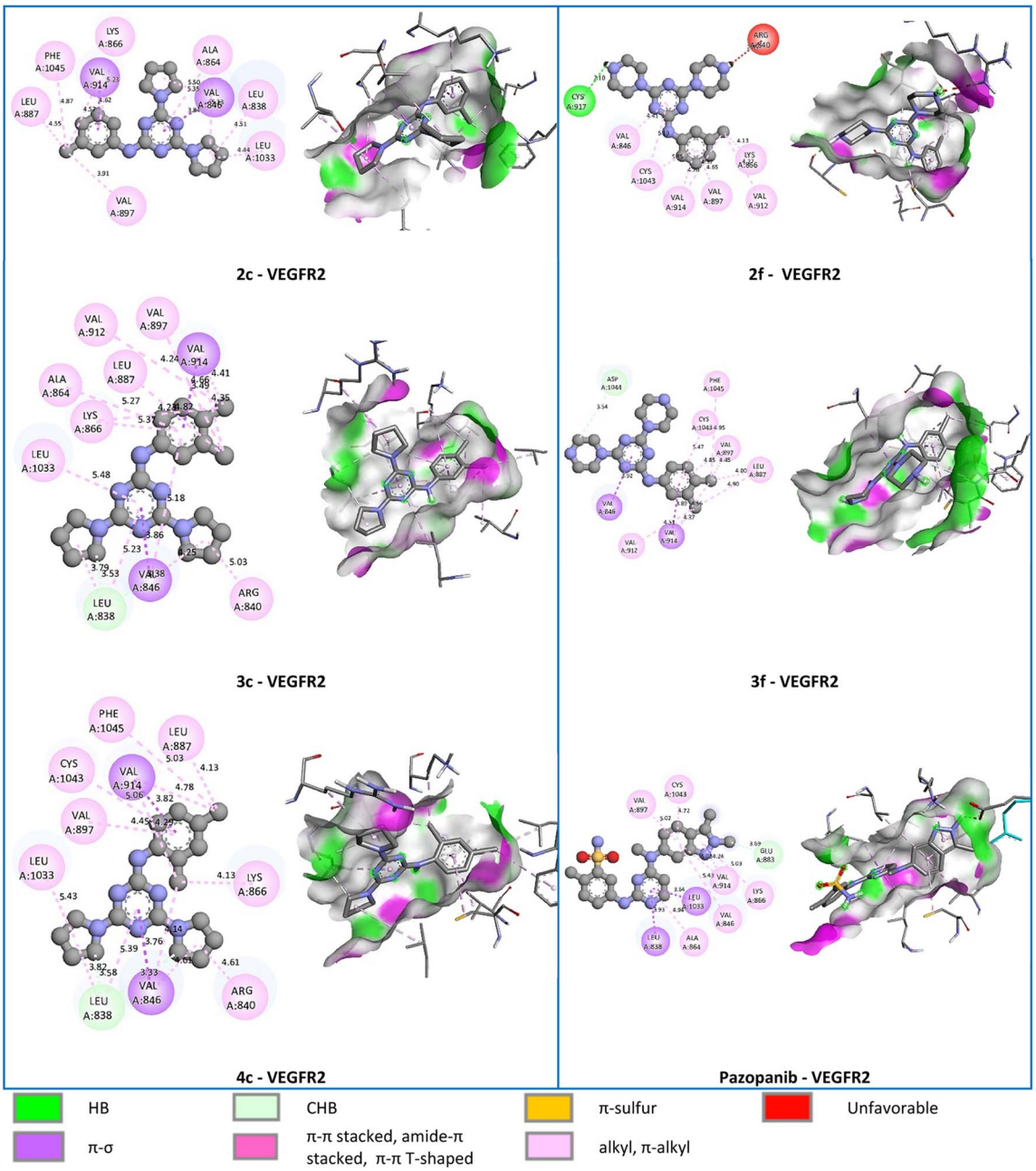

Fig. 5 2D and 3D representation of the interaction of potent chlorophenylamino-*s*-triazine derivatives and reference drug Pazopanib with vascular endothelial growth factor receptor 2 (VEGFR2) target.

including Lipinski, Ghose, Veber, Egan, Muegge, Pfizer, bioavailability score, and synthetic accessibility (SA) score. Compounds **2c**, **3c**, and **4c**, bearing pyrrolidine or dichlorophenyl substitutions, satisfy Lipinski, Ghose, Veber, Egan, and Muegge rules, indicating favorable molecular weight (<500 Da), lipophilicity ($\log P$ < 5), hydrogen bond donors/acceptors, and topological polar surface area (TPSA < 140 Å^2), aligning with characteristics of orally bioavailable drugs. However, these compounds fail the Pfizer rule, suggesting potential toxicity risks due to high lipophilicity or reactive groups, unlike Ged and Bim, which pass the Pfizer rule, indicating lower toxicity potential. Compounds **2f** and **3f**, with piperazine substitutions, also meet Lipinski, Veber, Egan, and Muegge criteria but fail the Ghose rule, which may limit their pharmacokinetic profiles compared to **2c**, **3c**, and **4c**. All five compounds achieve a bioavailability score of 0.55, matching Bim but surpassing Ged (0.17), suggesting comparable oral absorption potential to Bim, driven by favorable PSA and hydrogen bonding properties. The excellent SAscore across all compounds indicates synthetic feasibility, comparable to Ged and Bim, facilitating potential scale-up for clinical development. Overall, **2c**, **3c**, and **4c** exhibited superior druglikeness

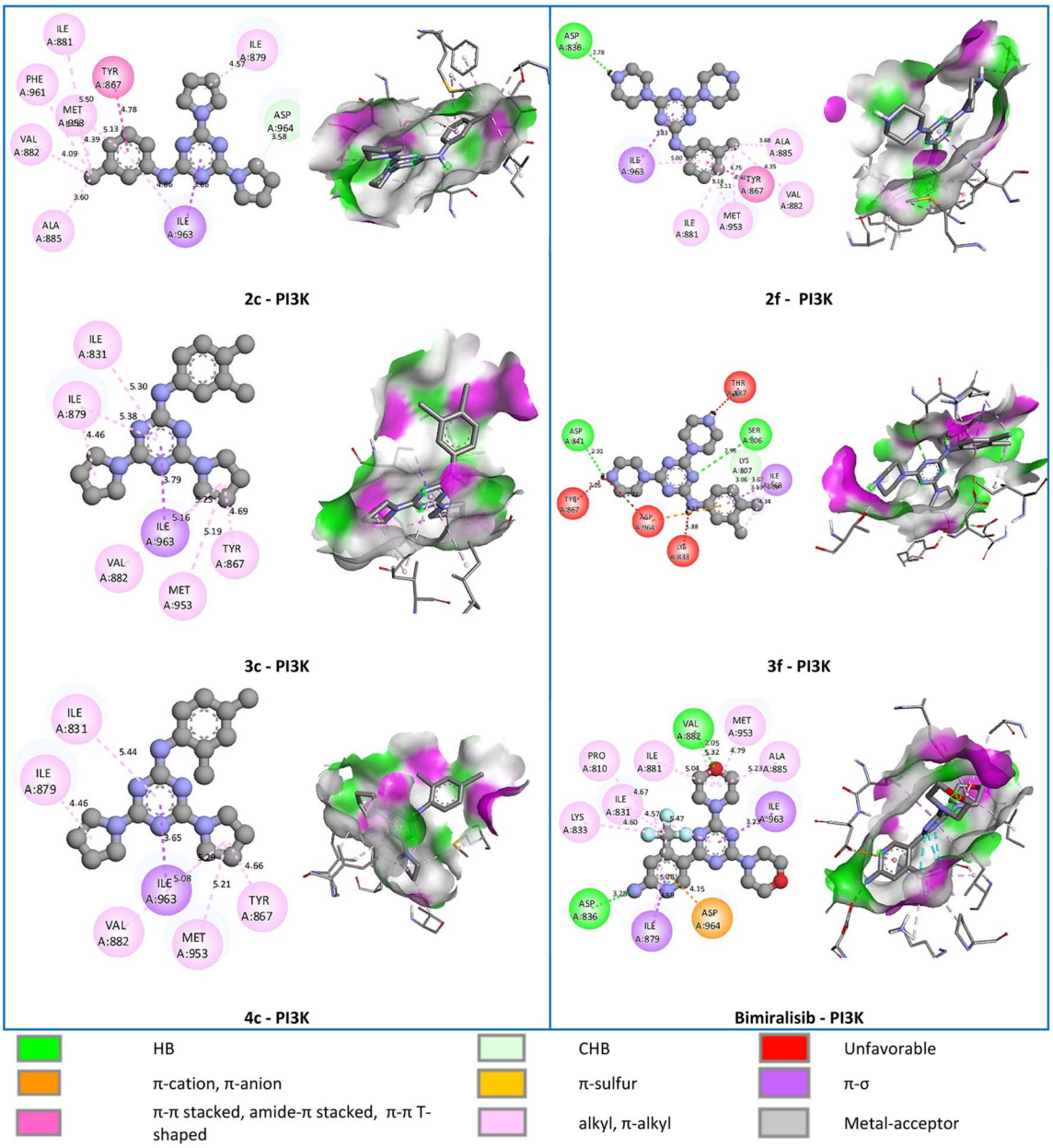

Fig. 6 2D and 3D representation of the interaction of potent chlorophenylamino-*s*-triazine derivatives and reference drug Bimiralisib with phosphoinositide 3-kinase (PI3K) target.

compared to Ged, with profiles comparable to Bim, though their Pfizer rule violations warrant further optimization to mitigate potential toxicity while maintaining their promising pharmacokinetic properties.

2.4.2. Adsorption. Compounds **2c**, **3c**, and **4c** exhibited excellent Caco-2 permeability ($\log P_{app}$: −4.883, −5.105, −4.942, respectively), comparable to Bim (−4.546) and superior to Ged (−5.322) and **2f** (−5.283), which are rated poor, suggesting

Table 5 Molecular docking targets for *in silico* studies

Entry	Target	Symbol	PDB ID	Organism	Expression system	Ref drug
1	Epidermal growth factor receptor	EGFR	3UG2	*Homo sapiens*	*Spodoptera frugiperda*	Gefitinib
2	Vascular endothelial growth factor receptor 2	VEGFR2	3CJG	*Homo sapiens*	*Spodoptera frugiperda*	Pazopanib
3	Phosphoinositide 3-kinase	PI3K	5OQ4	*Homo sapiens*	*Spodoptera frugiperda*	Bimiralisib

Table 6 Grid box parameters for anticancer targets

	Size			Center		
Target	*x*	*y*	*z*	*x*	*y*	*z*
EGFR	25	25	25	−0.1842	49.3505	20.0221
VEGFR2	25	25	25	8.1773	40.7893	7.3664
PI3K	25	25	25	43.1501	15.2623	32.1771

enhanced intestinal epithelial transport, likely due to favorable lipophilicity and molecular size. All compounds, including Ged and Bim, demonstrated excellent MDCK permeability, indicating efficient transcellular diffusion across renal epithelial cells. PAMPA results showed excellent permeability for **2c**, **2f**, **3c**, **4c**, Ged, and Bim, but **3f** is rated medium, possibly due to piperazine-induced polarity reducing membrane penetration. Regarding Pgp interactions, all compounds except **2f** and **3f** are poor Pgp inhibitors, similar to Ged and Bim, reducing the risk of drug–drug interactions, but **2f** and **3f** are excellent, suggesting potential inhibition that could enhance bioavailability of co-administered drugs. However, **2f** and **3f** are poor Pgp substrates, indicating efflux susceptibility, which may reduce their absorption compared to **2c**, **3c**, **4c**, and Bim (excellent substrates), while Ged is a poor substrate, potentially limiting its intestinal absorption. All compounds exhibited excellent HIA, $F_{20\%}$, and $F_{30\%}$, reflecting high intestinal absorption and bioavailability at lower doses, consistent with their favorable physicochemical profiles. However, **2c**, **2f**, **3c**, **3f**, and Ged show poor $F_{50\%}$ bioavailability, indicating reduced absorption at higher doses, possibly due to saturation of transport mechanisms, whereas **4c** and Bim achieved excellent $F_{50\%}$, suggesting robust dose-dependent absorption. Overall, **2c**, **3c**, and **4c** demonstrated superior absorption profiles, closely matching Bim and surpassing Ged, particularly in Caco-2 and $F_{50\%}$ metrics, though **2f** and **3f** are limited by poor substrate profiles and Caco-2 permeability, warranting structural optimization to enhance absorption.

2.4.3. Distribution. The distribution potential of five *s*-triazine derivatives (**2c**, **2f**, **3c**, **3f**, and **4c**) was evaluated against reference drugs Gedatolisib (Ged) and Bimiralisib (Bim) using key pharmacokinetic parameters, including plasma protein binding (PPB), volume of distribution at steady state (VDss), blood–brain barrier (BBB) penetration, fraction unbound (Fu), and inhibition of transporters (OATP1B1, OATP1B3, BCRP, MRP1, BSEP). Compounds **2c**, **3c**, and **4c** exhibit high PPB (99.60%, 99.60%, and 99.50%, respectively), rated poor, similar to Bim (94.20%), indicating extensive binding to plasma proteins, which may limit their free fraction available for tissue distribution. In contrast, **2f** and **3f** show lower PPB (78.00%, 79.50%), rated excellent, suggesting greater availability for tissue penetration, akin to Ged (76.5%). In addition, all compounds demonstrated excellent VDss with the optimal value ranging from 0.04 to 20 L kg^{-1} (**2c**: 3.546 L kg^{-1}, **2f**: 6.224 L kg^{-1}, **3c**: 4.144 L kg^{-1}, **3f**: 5.6750 L kg^{-1}, **4c**: 3.3880 L kg^{-1}, Ged: 2.6600 L kg^{-1}, Bim: 2.5760 L kg^{-1}), showed wide tissue distribution, likely driven by favorable lipophilicity. For BBB penetration, **2c** and Ged exhibited excellent profiles with BBB impermeability, while **2f**, **3c**, **3f**, **4c**, and Bim are poor or medium, possibly due to higher polarity or efflux transporter interactions. Fu values reflect PPB trends, with **2f** (20.50%) and **3f** (16.40%) showing excellent unbound fractions similar to Ged (18.0%), enhancing tissue distribution, compared to poor Fu for **2c** (0.30%), **3c** (0.30%), **4c** (0.40%), and Bim (6.30%). Moreover, all compounds are poor and medium inhibitors of OATP1B1, OATP1B3, BCRP, MRP1, and BSEP, similar to Ged and Bim. Overall, **2f** and **3f** exhibit superior distribution potential due to lower PPB and higher Fu, closely matching Ged, while **2c**, **3c**, and **4c** are limited by high PPB, akin to Bim, necessitating optimization to enhance free drug availability.

2.4.4. Metabolism. All compounds, including Ged and Bim, are potent CYP1A2 inhibitors, indicating potential drug–drug interactions with CYP1A2-metabolized drugs, such as theophylline. Compounds **2c**, **2f**, **3c**, **3f**, and **4c** are also CYP1A2 substrates, unlike Ged and Bim, suggesting susceptibility to metabolism *via* this enzyme, which may lead to variable clearance rates. For CYP2C19, only **3c** is an inhibitor of this enzyme, while **2f**, **3f**, **4c**, Ged, and Bim are substrates, implying potential metabolism by CYP2C19, which is potentially affected by genetic polymorphisms. Additionally, CYP2C9 inhibition is prominent in **2c**, **3c**, **3f**, and **4c**, with **2f** and Bim showing weaker inhibition, and Ged exhibiting none, indicating increased interaction risk for **2c**, **3c**, **3f**, and **4c** with CYP2C9-metabolized drugs like warfarin. CYP2D6 inhibition is observed in **2c** and **3c**, but none are substrates, similar to Ged and Bim, minimizing interactions with CYP2D6-metabolized drugs. Furthermore, CYP3A4, a major drug-metabolizing enzyme, is inhibited by **2f** and **3f**, and all triazines except **2c** are substrates, unlike Ged (weak substrate) and Bim (non-substrate), indicating potential for significant CYP3A4-mediated clearance in **2f**, **3f**, **3c**, and **4c**. CYP2B6 inhibition is seen in **2c**, **3c**, **4c**, and Ged, but none are substrates, reducing concerns for this pathway. CYP2C8 inhibition varies, with **2c** and **3c** showing strong inhibition and **2f** showing moderate inhibition, while **3f**, **4c**, Ged, and Bim are none. HLM stability is excellent for **4c**, medium for **2c** and **3c**, and poor for **2f**, **3f**, Ged, and Bim, showed that **4c** is highly resistant to hepatic metabolism, potentially leading to prolonged systemic exposure, while **2f** and **3f**'s poor stability suggests rapid clearance, akin to Ged and Bim. Overall, **4c** exhibits the most favorable metabolic profile with excellent HLM stability and broad CYP substrate activity, surpassing Ged and Bim, while **2f** and **3f**'s poor stability and extensive CYP interactions may limit their metabolic efficiency, necessitating optimization to balance clearance and interaction risks.

2.4.5. Excretion. Compounds **2c** (4.52 mL min^{-1} kg^{-1}), **2f** (4.222 mL min^{-1} kg^{-1}), **3c** (4.72 mL min^{-1} kg^{-1}), **3f** (4.293 mL min^{-1} kg^{-1}) exhibited low CL_{plasma} compared to **4c** (5.437 mL min^{-1} kg^{-1}), Ged (5.329 mL min^{-1} kg^{-1}) and Bim (5.41 mL min^{-1} kg^{-1}), which are rated medium due to slightly higher clearance rates that may reflect less favorable metabolic stability. The lower CL_{plasma} values of **2c**, **2f**, **3c**, and **3f** suggest a slightly slower clearance compared to **4c**, potentially allowing for prolonged systemic exposure, which could be advantageous for sustained therapeutic effects. Regarding $T_{1/2}$, all compounds

are ultra-short half-life drugs (0.5 to < 1 h). Compounds **3c** (0.82 h) and Bim (0.926 h) display the longest half-lives, indicating slower elimination and potentially longer duration of action, followed by **4c** (0.682 h), **3f** (0.65 h), **2c** (0.609 h), **2f** (0.47 h), and Ged (0.297 h). The shorter $T_{1/2}$ of Ged suggests rapid elimination, which may necessitate frequent dosing, whereas the *s*-triazine derivatives, particularly **3c**, balance efficient clearance with adequate residence time, aligning closely with Bim's favorable profile.

2.4.6. Toxicity. The toxicity profiles of five *s*-triazine derivatives were compared with reference drugs Ged and Bim across multiple parameters, including cardiotoxicity (hERG), hepatotoxicity (DILI, human hepatotoxicity), genotoxicity (AMES, carcinogenicity), and organ-specific toxicities. Compounds **2c**, **2f**, **3c**, **3f**, and **4c** showed medium to poor toxicity parameters including hERG blockers, hERG blockers (10 μm), DILI, FDAMDD, eye irritation, respiratory toxicity, human hepatotoxicity, drug-induced nephrotoxicity, drug-induced neurotoxicity, ototoxicity, genotoxicity, A549 cytotoxicity, and Hek293 cytotoxicity. Rat oral acute toxicity is excellent for **2c**, **3c**, **4c**, and Ged (0.202–0.289), but poor for **2f** and **3f** (0.720–0.756) and medium for Bim (0.428), suggesting safer acute profiles for pyrrolidine-substituted *s*-triazines. In addition, skin sensitization is excellent for **4c** and Bim (0.275–0.286), medium for **2c** and **3c**, and poor for **2f** and **3f** (0.922–0.932), suggesting piperazine groups increase sensitization risk. Carcinogenicity varies, with **2f** and **3f** (0.149–0.162, excellent) showing low risk, while **2c** and **3c** are medium, and **4c**, Ged, and Bim are poor (0.709–0.955), showing potential long-term safety concerns for **4c**. Compound **2c** exhibited low or no hepatotoxicity, while the remaining compounds including the reference drug exhibited moderate hematotoxicity. Moreover, bioaccumulation (BCF) and environmental toxicity (IGC50, LC50DM, LC50FM) show comparable values across compounds, with **4c** and **3c** slightly higher, indicating potential environmental persistence. In particular, all *s*-triazine compounds showed excellent toxicity parameters including AMES toxicity, eye corrosion, and RPMI-8226 immunotoxicity. Overall, **2c**, **3c**, and **4c** offer safer profiles in AMES, acute toxicity, and immunotoxicity compared to Ged and Bim, but their poor hERG, DILI, and organ-specific toxicities, particularly for **2f** and **3f**, necessitate structural optimization to mitigate risks.

2.5. Molecular docking

The present study screened *s*-triazine compounds with potent *in vitro* anticancer activity against three targets (EGFR – epidermal growth factor receptor, VEGFR2 – vascular endothelial growth factor receptor 2, and PI3K – phosphoinositide 3-kinase) to determine potential mechanisms of action similar to many other studies.[34–38] The binding affinity and bond information (bond type, bond length and amino acid residues) of the chlorophenylamino-*s*-triazine derivatives with three targets including EGFR, VEGFR2 and PI3K are shown in Table 4. The interactions of the symmetrical chlorophenylamino-*s*-triazine derivatives with amino acid residues at the active site of anticancer targets are shown in Fig. 4–6.

The binding affinities of the compounds (**2c**, **2f**, **3c**, **3f**, and **4c**) to EGFR, VEGFR2, and PI3K were evaluated against the reference drugs Gefitinib, Pazopanib, and Bimiralisib, respectively, to assess their inhibitory potential. For EGFR, five compounds exhibited binding affinities ranging from −7.4 to −7.8 kcal mol^{-1}, surpassing Gefitinib's −7.3 kcal mol^{-1}. Compounds **2f** and **3f** showed the highest affinity at −7.8 kcal mol^{-1}, followed by **4c** (−7.7 kcal mol^{-1}), **3c** (−7.6 kcal mol^{-1}), and **2c** (−7.4 kcal mol^{-1}), indicating a slight but consistent improvement over Gefitinib. For VEGFR2, five compounds showed the binding affinities range from −8.6 to −9.1 kcal mol^{-1}, approaching but not exceeding Pazopanib's −10.0 kcal mol^{-1}. Compound **3c** showed the highest affinity (−9.1 kcal mol^{-1}), followed by **2f** and **3f** (−8.9 kcal mol^{-1}), **2c** (−8.8 kcal mol^{-1}), and **4c** (−8.6 kcal mol^{-1}), suggesting robust but slightly weaker binding compared to Pazopanib. For PI3K, potent compounds exhibited binding affinities range from −8.6 to −9.0 kcal mol^{-1}, closely matching Bimiralisib's −9.1 kcal mol^{-1}. Compound **2f** (−9.0 kcal mol^{-1}) nearly equals Bimiralisib, followed by **2c** and **3f** (−8.8 kcal mol^{-1}), and **3c** and **4c** (−8.6 kcal mol^{-1}), indicating high potency across all compounds. These results highlighted **2f** and **3c** as consistently strong binders across all three targets, closely rivaling the reference drugs.

At the EGFR active site, Gefitinib binds to EGFR with an affinity of −7.3 kcal mol^{-1}, forming one hydrogen bond (HB) with ASP855 (3.54 Å), one π-sulfur interaction with MET790 (3.56 Å), and eight hydrophobic interactions with LEU718, VAL726, ALA743, LEU844, and LYS745 (3.83–5.48 Å). Compound **2c** (−7.4 kcal mol^{-1}) mirrored Gefitinib's π-sulfur interaction with MET790 (3.52 Å) and shared hydrophobic interactions with LEU718, ALA743, LEU844, LYS745, and VAL726, supplemented by additional hydrophobic contacts with CYS797 and LEU788, enhancing its binding network. Compound **2f** (−7.8 kcal mol^{-1}) formed two HBs with GLU762 (2.27 Å) and THR854 (3.48 Å), which are absent in Gefitinib, and shared hydrophobic interactions with LEU718, LEU844, and ALA743, suggesting a more diverse interaction profile. Compound **3c** (−7.6 kcal mol^{-1}) relies on eight hydrophobic interactions, overlapping with Gefitinib at LEU718, LYS745, MET790, LEU844, and ALA743, but lacks polar interactions, potentially limiting its specificity. Compound **3f** (−7.8 kcal mol^{-1}) formed one HB with GLU762 (2.85 Å), a unique feature, and shared hydrophobic interactions with LEU718, LEU844, and ALA743. Compound **4c** (−7.7 kcal mol^{-1}) formed 12 hydrophobic interactions, including LEU718, ALA743, LYS745, MET790, VAL726, and LEU844, closely resembling Gefitinib's hydrophobic profile but lacking polar interactions. The shared interactions with MET790, LEU718, LEU844, and ALA743 across all compounds indicate a conserved EGFR binding pocket, with **2f** and **3f** introducing unique polar contacts.

At the VEGFR2 active site, Pazopanib binded to VEGFR2 with an affinity of −10.0 kcal mol^{-1}, forming one HB with GLU883 (3.69 Å) and nine hydrophobic interactions with LEU838, LEU1033, LYS866, VAL914, ALA864, VAL846, VAL897, and CYS1043 (3.64–5.43 Å). Compound **2c** (−8.8 kcal mol^{-1}) formed 13 hydrophobic interactions, sharing VAL846, VAL914, LEU838,

LEU1033, LYS866, VAL897, and CYS1043 with Pazopanib, but lacks polar interactions, which may explain its lower affinity. Compound **2f** (−8.9 kcal mol^{-1}) formed one HB with CYS917 (2.10 Å), absent in Pazopanib, and shared hydrophobic interactions with VAL846, VAL914, LYS866, VAL897, and CYS1043, suggesting a partially conserved binding mode. Compound **3c** (−9.1 kcal mol^{-1}) formed two HBs with LEU838 (3.53 Å) and VAL846 (3.38 Å) and 16 hydrophobic interactions, including VAL846, VAL914, LEU838, LYS866, VAL897, LEU1033, and CYS1043, closely resembling Pazopanib's profile while adding polar interactions for enhanced stability. Compound **3f** (−8.9 kcal mol^{-1}) formed one HB with ASP1044 (3.54 Å) and 11 hydrophobic interactions, sharing VAL846, VAL914, LEU887, VAL897, and CYS1043 with Pazopanib. Compound **4c** (−8.6 kcal mol^{-1}) formed two HBs with LEU838 (3.60 Å) and VAL846 (3.33 Å) and 15 hydrophobic interactions, overlapping with Pazopanib at VAL846, VAL914, LEU838, LEU1033, LYS866, VAL897, and CYS1043. The shared hydrophobic interactions with VAL846, VAL914, LYS866, and VAL897 across all compounds indicate a conserved binding site, with **3c** and **4c** introducing additional HBs to enhance binding.

At the PI3K active site, Bimiralisib binded to PI3K with an affinity of −9.1 kcal mol^{-1}, forming two HBs with VAL882 (2.05 Å) and ASP836 (3.28 Å), one electrostatic interaction with ASP964 (4.15 Å), and 11 hydrophobic interactions with VAL882, ILE879, ILE963, ILE881, ALA885, MET953, and ILE831 (3.59–5.47 Å). Compound **2c** (−8.8 kcal mol^{-1}) formed one HB with ASP964 (3.58 Å) and 10 hydrophobic interactions, sharing VAL882, ILE879, ILE963, ALA885, and MET953 with Bimiralisib, indicating a similar binding mode. Compound **2f** (−9.0 kcal-mol^{-1}) formed one HB with ASP836 (2.78 Å), mirroring Bimiralisib's interaction, and shared hydrophobic interactions with VAL882, ILE963, ALA885, and MET953, suggesting high similarity. Compound **3c** (−8.7 kcal mol^{-1}) showed eight hydrophobic interactions, overlapping with Bimiralisib at VAL882, ILE879, ILE963, MET953, and ILE831, but lacks polar interactions. Compound **3f** (−8.8 kcal mol^{-1}) formed two HBs with SER806 (2.96 Å) and ASP841 (2.91 Å), one electrostatic interaction with ASP964 (4.19 Å), one π-donor HB with LYS807 (3.06 Å), and five hydrophobic interactions, sharing ASP964 with Bimiralisib while introducing unique polar contacts. Compound **4c** (−8.6 kcal mol^{-1}) formed seven hydrophobic interactions, overlapping with Bimiralisib at VAL882, ILE879, ILE963, MET953, and ILE831, but lacks polar interactions. The shared hydrophobic interactions with VAL882, ILE963, and MET953 across all compounds highlight a conserved PI3K binding pocket, with **2f** and **3f** closely mimicking Bimiralisib's polar interactions.

In summary, compounds **2f** and **3c** stand out as the most promising candidates for multi-targeted inhibition of EGFR, VEGFR2, and PI3K, based on their robust binding affinities and interaction profiles, which closely rival or approach those of the reference drugs Gefitinib, Pazopanib, and Bimiralisib. For EGFR, **2f** showed the highest affinity (−7.8 kcal mol^{-1}), surpassing Gefitinib (−7.3 kcal mol^{-1}), with unique hydrogen bonds to GLU762 and THR854, alongside hydrophobic interactions with LEU718, LEU844, and ALA743, suggesting enhanced binding specificity. Compound **3c** (−7.6 kcal mol^{-1}) also outperformed Gefitinib, sharing key hydrophobic interactions with MET790, LEU718, and LEU844. For VEGFR2, **3c** exhibited the highest affinity (−9.1 kcal mol^{-1}), closely approaching Pazopanib (−10.0 kcal mol^{-1}), with two hydrogen bonds (LEU838, VAL846) and an extensive hydrophobic network (VAL846, VAL914, LYS866, VAL897), indicating strong binding stability. Compound **2f** (−8.9 kcal mol^{-1}) complemented this with a hydrogen bond to CYS917 and shared hydrophobic interactions, reinforcing its potency. For PI3K, **2f** (−9.0 kcal mol^{-1}) nearly matches Bimiralisib (−9.1 kcal mol^{-1}), with a hydrogen bond to ASP836 and hydrophobic interactions with VAL882, ILE963, and MET953, closely mimicking Bimiralisib's profile. Compound **3f** (−8.8 kcal mol^{-1}) also showed promise with diverse polar interactions (SER806, ASP841, ASP964, LYS807), though **2f**'s closer affinity to Bimiralisib gives it an edge. While **2c**, **3f**, and **4c** demonstrated competitive affinities and interactions, **2f** and **3c** consistently excel across all targets due to their high affinities and balanced polar and hydrophobic interactions, making them prime candidates for further optimization as multi-targeted kinase inhibitors.

3. Conclusion

In conclusion, this study advanced the development of symmetrical chlorophenylamino-*s*-triazine derivatives as potent anticancer agents, building upon our prior investigation of symmetrical di-substituted phenylamino-*s*-triazine analogs. By synthesizing 20 compounds *via* microwave-assisted (MW) and reflux (RF) methods, MW achieved superior yields (88–95%) and markedly reduced reaction times compared to RF (78–86%), echoing the efficiency gains observed in the earlier work where MW similarly outperformed reflux with yields exceeding 90%. Compounds **2c** (3-Cl, pyrrrolidine), **2f** (3-Cl, piperazine), **3c** (3,4-diCl, pyrrrolidine), **3f** (3,4-diCl, piperazine), and **4c** (2,4-diCl, pyrrrolidine) exhibited significant cytotoxic potential (IC_{50} < 12 μM) against both MCF7 and C26 cell lines, with **4c** (featuring 2,4-dichlorophenyl and pyrrolidine moieties; IC_{50} = 1.71 μM) surpassing paclitaxel. These results represented a substantial improvement over the previously most active derivatives, which achieved IC_{50} values below 15 μM against C26 lines but relied on morpholino and mono-substituted halogen or nitro groups. This enhanced potency in the current series underscored the synergistic role of pyrrolidine's lipophilicity and dichlorophenyl's electron-withdrawing effects, as confirmed by QSAR analysis, extending SAR from the previous emphasis on 4-halogeno or 4-nitro substituents and morpholino scaffolds. Pharmacokinetically, **2c**, **3c**, and **4c** demonstrated absorption profiles comparable to Bimiralisib and superior to Gefitinib, with **4c** showing exceptional metabolic stability. However, challenges such as high plasma protein binding and potential toxicities (*e.g.*, hERG inhibition and drug-induced liver injury in **2f** and **3f**) mirror some limitations in the prior compounds, though the current derivatives exhibit lower toxicity on normal cells, akin to the selective profiles of previously phenylamino-*s*-triazine analogs relative to doxorubicin. Molecular docking further positions **2f** and **3c** as promising multi-targeted kinase

inhibitors, with binding affinities (−7.8 to −9.1 kcal mol^{-1}) rivaling Gefitinib, Pazopanib, and Bimiralisib across EGFR, VEGFR2, and PI3K – expanding the multi-target interactions (including DHFR, CDK2, and mTOR) identified in the earlier docking studies. Overall, these findings highlight the synthetic and therapeutic optimizations in this new series, offering greater potency and drug-like properties than their di-substituted predecessors. Future efforts should prioritize structural refinements to mitigate toxicity, bolster efficacy against various cancer cell lines, and validate mechanisms through kinase inhibition assays and *in vivo* models, thereby accelerating the translational potential of these *s*-triazine derivatives toward clinical anticancer applications.

4. Experimental section

4.1. Materials

All reagents and solvents were sourced from reputable commercial suppliers, including Merck and Acros Organics, ensuring high purity and homogeneity. Thin-layer chromatography (TLC) was performed using pre-coated silica gel aluminum plates (60 GF254, Merck), with visualization achieved under shortwave ultraviolet light at 254 nm. For purification, column chromatography was performed using high-grade silica gel (0.040–0.063 mm, Merck).

Microwave-assisted reactions were performed in a CEM Discover Microwave Synthesizer (USA), equipped with a magnetic stirrer for thorough mixing and an infrared sensor for precise temperature monitoring and control. Melting points were determined using a Sanyo–Gallenkamp apparatus, providing accurate thermal characterization. Nuclear magnetic resonance (NMR) spectra were obtained on a Bruker Avance 600/500 spectrometer, with chemical shifts reported in parts per million (δ, ppm) relative to standard references. High-resolution mass spectrometry was performed on an Agilent Series 1100 LC-MS trap system, ensuring accurate molecular weight determination. Finally, the optical density (*A*) was measured at 570 nm on a MultiskanTM microplate reader in the anti-cancer activity assay.

4.2. Experimental procedures

4.2.1 General procedure for synthesizing mono-substituted *s*-triazine derivatives (1a–1c). Cyanuric chloride (7.5 mmol) was dissolved in tetrahydrofuran (THF, 15 mL) and cooled to 0–5 °C. Subsequently, monochloro and dichloro aniline derivatives (5 mmol) and potassium carbonate (K_2CO_3, 5 mmol) were gradually added to the solution. The reaction mixture was stirred continuously and monitored by TLC until complete consumption of the aromatic amine was observed (typically 30–60 min). Upon completion, THF was evaporated under reduced pressure using a Heidolph rotary evaporator.[23] The resulting crude product was purified *via* recrystallization from a 1 : 1 (v/v) ethanol–water mixture, yielding the desired mono-substituted *s*-triazine derivatives in excellent yields of 95–97%.

4,6-Dichloro-N-(3-chlorophenyl)-1,3,5-triazin-2-amine ***(1a).*** White solid, yield 97%, mp 144–146 °C. ^{1}H NMR (500 MHz, DMSO-d_6, δ ppm): 11.28 (1H, s, –NH–), 7.73 (1H, t, J = 2.0 Hz, H_{Ar}), 7.21–7.19 (1H, m, H_{Ar}), 7.40 (1H, t, J = 7.0 Hz, H_{Ar}), 7.56–7.55 (1H, m, H_{Ar}). ^{13}C NMR (125 MHz, DMSO-d_6, δ ppm): 163.2, 162.7, 142.5, 132.6, 129.8, 120.3, 118.4, 117.2.

4,6-Dichloro-N-(3,4-dichlorophenyl)-1,3,5-triazin-2-amine ***(1b).*** White solid, yield 96%, mp 152–154 °C. ^{1}H NMR (500 MHz, DMSO-d_6, δ ppm): 10.87 (1H, s, –NH–), 8.02 (1H, d, J = 2.0 Hz, H_{Ar}), 7.61 (1H, d, J = 7.5 Hz, H_{Ar}), 7.47 (1H, dd, J = 7.5, 2.0 Hz, H_{Ar}). ^{13}C NMR (125 MHz, DMSO-d_6, δ ppm): 153.9, 137.7, 131.0, 130.7, 125.7, 122.1, 120.9.

4,6-Dichloro-N-(2,4-dichlorophenyl)-1,3,5-triazin-2-amine ***(1c).*** White solid, yield 95%, mp 149–151 °C. ^{1}H NMR (500 MHz, DMSO-d_6, δ ppm): 11.02 (1H, s, –NH–), 7.76 (1H, d, J = 2.0 Hz), 7.56 (1H, d, J = 7.0 Hz, H_{Ar}), 7.52 (1H, dd, J = 7.5, 2.0 Hz, H_{Ar}). ^{13}C NMR (125 MHz, DMSO-d_6, δ ppm): 165.2, 152.5, 134.4, 129.8, 128.9, 128.0, 127.7, 127.5.

4.2.2 General procedure for the preparation of chloro-phenylamino-*s*-triazine derivatives (2a–2g, 3a–3g and 4a–4f)

The reflux method. A series of mono-substituted *s*-triazine derivatives **1a–1c** (5 mmol) was synthesized by reacting with a saturated amine (15 mmol) in the presence of potassium carbonate (10 mmol) as a base in 1,4-dioxane (30 mL). The reaction mixture was refluxed for 12–24 h until completion, as monitored by thin-layer chromatography (TLC). Upon completion, the solvent was evaporated under reduced pressure using a Heidolph rotary evaporator to yield a crude solid.[23] Purification was achieved either by recrystallization from an ethanol : water mixture (2 : 8, v/v) or by column chromatography on silica gel with a hexane : ethyl acetate eluent system. Reaction yields range from 78 to 86%.

Microwave-assisted synthesis method. A mixture of the mono-substituted *s*-triazine derivatives **1a–1c** (5 mmol), saturated amine (15 mmol), and potassium carbonate (10 mmol) in 1,4-dioxane (10 mL) was subjected to microwave irradiation in a synthesizer at a fixed power of 300 W and a temperature of 105 °C. The reaction was monitored by TLC and typically completed within 15–30 min. The 1,4-dioxane was then removed under reduced pressure using a Heidolph rotary evaporator.[23] Purification of the crude product was achieved through recrystallization from an ethanol–water mixture (2 : 8, v/v) or column chromatography on silica gel using a hexane–ethyl acetate eluent. Reaction yields range from 88 to 95%.

Purity. All compounds have shown high purity, which was assessed by high-resolution ^{1}H-NMR (500 MHz).

Solubility profile. The synthesized tri-substituted *s*-triazine derivatives exhibited high solubility in polar solvents such as dimethyl sulfoxide (DMSO), 1,4-dioxane, and methanol. In addition, these compounds exhibited moderate solubility in ethanol and water but limited solubility in nonpolar solvents (*e.g.*, hexane and ethyl acetate).

Stability characteristics. The synthesized compounds showed excellent stability at room temperature. For long-term storage, it is recommended to maintain these compounds at 4–8 °C to preserve their integrity.

N-(3-Chlorophenyl)-4,6-di(piperidin-1-yl)-1,3,5-triazin-2-amine ***(2a)***. White solid, mp 131–133 °C. ^{1}H NMR (500 MHz, DMSO-d_6, δ ppm): 9.14 (1H, s, –NH–), 7.99 (1H, t, J = 1.5 Hz, H_{Ar}), 7.54 (1H, d, J = 6.5 Hz, H_{Ar}), 7.24 (1H, t, J = 7.0 Hz, H_{Ar}), 6.93 (1H, dd, J = 7.0, 1.0 Hz, H_{Ar}), 3.70 (8H, t, J = 4.5 Hz, –CH_2–), 1.61 (4H, d, J = 4.0 Hz, –CH_2–), 1.49 (8H, d, J = 3.0 Hz, –CH_2–). ^{13}C NMR (125 MHz, DMSO-d_6, δ ppm): 164.3, 164.0, 142.2, 132.7, 129.8, 120.5, 118.6, 117.4, 43.6, 25.3, 24.3. LC-MS (m/z) $[M + H]^+$ calcd for $C_{19}H_{26}ClN_6$ 373.1902, found 373.1910.

N-(3-Chlorophenyl)-4,6-bis(4-methylpiperidin-1-yl)-1,3,5-triazin-2-amine ***(2b)***. White solid, mp 164–166 °C. ^{1}H NMR (500 MHz, DMSO-d_6, δ ppm): 9.16 (1H, s, –NH–), 8.01 (1H, s, H_{Ar}), 6.92 (1H, dd, J = 6.5, 1.0 Hz, H_{Ar}), 7.23 (1H, t, J = 7.0 Hz, H_{Ar}), 7.53 (1H, d, J = 7.0 Hz, H_{Ar}), 4.60 (4H, d, J = 11 Hz, –CH_2–), 2.79 (4H, t, J = 10 Hz, –CH_2–), 1.02 (4H, q, J = 10.5 Hz, –CH_2–), 1.64–1.58 (6H, m, –CH_2– and –CH<), 0.89 (6H, d, J = 5.0 Hz, –CH_3). ^{13}C NMR (125 MHz, DMSO-d_6, δ ppm): 164.3, 164.0, 142.2, 132.7, 129.8, 120.4, 118.6, 117.3, 43.0, 33.6, 30.6, 21.7. LC-MS (m/z) $[M + H]^+$ calcd for $C_{21}H_{30}ClN_6$ 401.2215, found 401.2197.

N-(3-Chlorophenyl)-4,6-di(pyrrolidin-1-yl)-1,3,5-triazin-2-amine ***(2c)***. White solid, mp 120–122 °C. ^{1}H NMR (500 MHz, DMSO-d_6, δ ppm): 9.13 (1H, s, –NH–), 8.16 (1H, t, J = 2.0 Hz, H_{Ar}), 7.66 (1H, dd, J = 7.0, 1.5 Hz, H_{Ar}), 7.22 (1H, t, J = 7.0 Hz, H_{Ar}), 6.90 (1H, dd, J = 7.0, 2.0 Hz, H_{Ar}), 3.47 (8H, t, J = 5.5 Hz, –CH_2–), 1.87 (8H, s, –CH_2–). ^{13}C NMR (125 MHz, DMSO-d_6, δ ppm): 163.4, 163.0, 142.6, 132.7, 129.8, 120.2, 118.5, 117.5, 45.6, 24.8. LC-MS (m/z) $[M + H]^+$ calcd for $C_{17}H_{22}ClN_6$ 345.1549, found 345.1587.

N-(3-Chlorophenyl)-4,6-dimorpholino-1,3,5-triazin-2-amine ***(2d)***. White solid, mp 200–201 °C. ^{1}H NMR (500 MHz, DMSO-d_6, δ ppm): 9.31 (1H, s, –NH–), 7.88 (1H, t, J = 1.5 Hz, H_{Ar}), 7.61 (1H, dd, J = 7.0, 1.0 Hz, H_{Ar}), 7.26 (1H, t, J = 7.5 Hz, H_{Ar}), 6.93 (1H, dd, J = 7.0, 1.5 Hz, H_{Ar}), 3.70 (8H, t, J = 4.5 Hz, –CH_2–), 3.62 (8H, d, J = 4.0 Hz, –CH_2–). ^{13}C NMR (125 MHz, DMSO-d_6, δ ppm): 164.6, 163.9, 141.9, 132.7, 129.9, 120.8, 118.8, 117.7, 66.3, 43.3. LC-MS (m/z) $[M + H]^+$ calcd for $C_{17}H_{22}ClN_6O_2$ 377.1487, found 377.1489 $[M - H]^-$ calcd for $C_{17}H_{20}ClN_6O_2$ 375.1342; found 375.1324.

N-(3-Chlorophenyl)-4,6-bis(4-methylpiperazin-1-yl)-1,3,5-triazin-2-amine ***(2e)***. White solid, mp 166–168 °C. ^{1}H NMR (500 MHz, DMSO-d_6, δ ppm): 9.25 (1H, s, –NH–), 7.91 (1H, d, J = 2.0 Hz, H_{Ar}), 6.94 (1H, dd, J = 6.5, 1.0 Hz, H_{Ar}), 7.25 (1H, q, J = 7.0 Hz, H_{Ar}), 7.55 (1H, dd, J = 7.0, 1.0 Hz, H_{Ar}), 3.81–3.70 (8H, m, –CH_2–), 2.31 (8H, t, J = 4.0 Hz, –CH_2–), 2.18 (6H, s, –CH_3). ^{13}C NMR (125 MHz, DMSO-d_6, δ ppm): 164.3, 164.1, 142.3, 132.7, 129.8, 120.4, 118.6, 117.3, 43.0, 33.6, 30.6. LC-MS (m/z) $[M + H]^+$ calcd for $C_{19}H_{28}ClN_8$ 403.2120, found 403.2131.

N-(3-Chlorophenyl)-4,6-di(piperazin-1-yl)-1,3,5-triazin-2-amine ***(2f)***. White solid, mp 241–243 °C. ^{1}H NMR (500 MHz, DMSO-d_6, δ ppm): 9.29 (1H, s, –NH–), 7.94 (1H, d, J = 1.5 Hz, H_{Ar}), 7.57 (1H, dd, J = 6.5, 1.0 Hz, H_{Ar}), 7.27 (1H, q, J = 7.0 Hz, H_{Ar}), 6.96 (1H, dd, J = 6.5, 1.0 Hz, H_{Ar}), 3.85–3.80 (4H, m, –CH_2–), 3.68 (4H, t, J = 4.0 Hz, –CH_2–), 2.72 (4H, s, –CH_2–), 2.51–2.50 (4H, m, –CH_2–). ^{13}C NMR (125 MHz, DMSO-d_6, δ ppm): 164.4, 163.9, 142.0, 132.7, 129.9, 120.7, 118.8, 117.6, 44.2, 42.6. LC-MS (m/z) $[M + H]^+$ calcd for $C_{17}H_{24}ClN_8$ 375.1807, found 375.1811.

N^2-(3-Chlorophenyl)-N^4,N^4,N^6,N^6-tetraethyl-1,3,5-triazine-2,4,6-triamine ***(2g)***. White solid, mp 125–127 °C. ^{1}H NMR (600 MHz, DMSO-d_6, δ ppm): 10.76 (1H, s, –NH–), 8.02 (1H, s, H_{Ar}), 7.41–7.36 (2H, m, H_{Ar}), 7.14 (1H, d, J = 7.2 Hz, H_{Ar}), 3.93–3.57 (8H, m, –CH_2–), 1.27–1.16 (12H, m, –CH_3). ^{13}C NMR (125 MHz, DMSO-d6, δ ppm): 139.5, 133.2, 130.4, 122.9, 119.3, 118.0, 42.0, 13.1. LC-MS (m/z) $[M + H]^+$ calcd for $C_{17}H_{26}N_6Cl$ 349.1902, found 349.1880.

N-(3,4-Dichlorophenyl)-4,6-di(piperidin-1-yl)-1,3,5-triazin-2-amine ***(3a)***. White solid, mp 142–144 °C. ^{1}H NMR (500 MHz, DMSO-d_6, δ ppm): 9.07 (1H, s, –NH–), 8.18 (1H, d, J = 2.0 Hz, H_{Ar}), 7.58 (1H, dd, J = 7.5, 2.0 Hz, H_{Ar}), 7.43 (1H, d, J = 7.0 Hz, H_{Ar}), 3.70 (8H, t, J = 4.5 Hz, –CH_2–), 1.63 (4H, t, J = 4.5 Hz, –CH_2–), 1.51 (8H, d, J = 4.5 Hz, –CH_2–). ^{13}C NMR (125 MHz, DMSO-d_6, δ ppm): 165.0, 164.6, 141.5, 131.0, 130.4, 122.8, 121.0, 119.7, 44.3, 25.8, 24.8. LC-MS (m/z) $[M + H]^+$ calcd for $C_{19}H_{25}Cl_2N_6$ 407.1512, found 407.1503 $[M - H]^-$ calcd for $C_{19}H_{23}Cl_2N_6$ 405.1367, found 405.1356.

N-(3,4-Dichlorophenyl)-4,6-bis(4-methylpiperidin-1-yl)-1,3,5-triazin-2-amine ***(3b)***. White solid, mp 167–169 °C. ^{1}H NMR (500 MHz, DMSO-d_6, δ ppm): 9.28 (1H, s, –NH–), 8.20 (1H, d, J = 2.5 Hz, H_{Ar}), 7.55 (1H, dd, J = 7.5, 2.0 Hz, H_{Ar}), 7.45 (1H, d, J = 7.5 Hz, H_{Ar}), 4.59 (4H, d, J = 10.5 Hz, –CH_2–), 2.81 (4H, t, J = 10 Hz, –CH_2–), 1.64–1.58 (6H, m, –CH_2– and –CH<), 1.01 (4H, q, J = 10.5 Hz, –CH_2–), 0.90 (6H, d, J = 5.5 Hz, –CH_3). ^{13}C NMR (125 MHz, DMSO-d_6, δ ppm): 164.3, 163.9, 140.9, 130.5, 130.0, 122.1, 120.2, 119.0, 43.0, 33.5, 30.6, 21.7. LC-MS (m/z) $[M + H]^+$ calcd for $C_{21}H_{29}Cl_2N_6$ 435.1825, found 435.1827.

N-(3,4-Dichlorophenyl)-4,6-di(pyrrolidin-1-yl)-1,3,5-triazin-2-amine ***(3c)***. White solid, mp 126–128 °C. ^{1}H NMR (500 MHz, DMSO-d_6, δ ppm): 9.03 (1H, s, –NH–), 8.35 (1H, d, J = 2.0 Hz, H_{Ar}), 7.69 (1H, dd, J = 7.0, 2.0 Hz, H_{Ar}), 7.41 (1H, d, J = 7.5 Hz, H_{Ar}), 3.49 (8H, t, J = 5.5 Hz, –CH_2–), 1.90 (8H, t, J = 5.5 Hz, –CH_2–). ^{13}C NMR (125 MHz, DMSO-d_6, δ ppm): 163.1, 162.8, 141.0, 130.2, 129.5, 121.7, 120.1, 118.7, 45.3, 24.4. LC-MS (m/z) $[M + H]^+$ calcd for $C_{17}H_{21}Cl_2N_6$ 379.1199, found 379.1179 $[M - H]^-$ calcd for $C_{17}H_{19}Cl_2N_6$ 377.1054, found 377.1061.

N-(3,4-Dichlorophenyl)-4,6-dimorpholino-1,3,5-triazin-2-amine ***(3d)***. White solid, mp 208–210 °C. ^{1}H NMR (500 MHz, DMSO-d_6, δ ppm): 9.41 (1H, s, –NH–), 8.06 (1H, d, J = 2.5 Hz, H_{Ar}), 7.62 (1H, dd, J = 7.5, 2.0 Hz, H_{Ar}), 7.47 (1H, d, J = 7.5 Hz, H_{Ar}), 3.70 (8H, t, J = 4.0 Hz, –CH_2–), 3.62 (8H, d, J = 4.0 Hz, –CH_2–). ^{13}C NMR (125 MHz, DMSO-d_6, δ ppm): 164.5, 163.8, 140.6, 130.5, 130.2, 122.5, 120.5, 119.3, 66.3, 43.3. LC-MS (m/z) $[M + H]^+$ calcd for $C_{17}H_{21}Cl_2N_6O_2$ 411.1098, found 411.1095 $[M - H]^-$ calcd for $C_{17}H_{18}Cl_2N_6O_2$ 409.0952, found 409.0955.

N-(3,4-Dichlorophenyl)-4,6-bis(4-methylpiperazin-1-yl)-1,3,5-triazin-2-amine ***(3e)***. White solid, mp 174–76 °C. ^{1}H NMR (500 MHz, DMSO-d_6, δ ppm): 9.35 (1H, s, –NH–), 8.10 (1H, d, J = 2.0 Hz, H_{Ar}), 7.59 (1H, dd, J = 7.5, 2.0 Hz, H_{Ar}), 7.48 (1H, d, J = 7.5 Hz, H_{Ar}), 3.71 (8H, t, J = 4.0 Hz, –CH_2), 2.33 (8H, t, J = 4.0 Hz, –CH_2–), 2.20 (6H, s, –CH_3). ^{13}C NMR (125 MHz, DMSO-d_6, δ ppm): 164.6, 164.0, 140.8, 130.7, 130.4, 122.7, 120.6, 119.4, 54.5, 45.4, 42.5. LC-MS (m/z) $[M + H]^+$ calcd for $C_{19}H_{27}Cl_2N_8$ 437.1730, found 437.1721.

*N-(3,4-Dichlorophenyl)-4,6-di(piperazin-1-yl)-1,3,5-triazin-2-amine (**3f**).* White solid, mp 249–251 °C. ^{1}H NMR (500 MHz, DMSO-d_6, δ ppm): 9.17 (1H, s, –NH–), 8.14 (1H, d, J = 2.0 Hz, H_{Ar}), 7.62 (1H, dd, J = 9.0, 2.0 Hz, H_{Ar}), 7.46 (1H, d, J = 9.0 Hz, H_{Ar}), 3.85–3.81 (4H, m, –CH_2–), 3.69–3.64 (4H, m, –CH_2–), 2.78–2.69 (4H, m, –CH_2–), 2.51–2.49 (4H, m, –CH_2–). ^{13}C NMR (125 MHz, DMSO-d_6, δ ppm): 164.5, 164.3, 163.7, 140.4, 130.2, 129.7, 122.3, 120.4, 119.1, 44.1, 42.4. LC-MS (m/z) $[M + H]^+$ calcd for $C_{17}H_{23}Cl_2N_8$ 409.1417, found 409.1422.

*N^2-(3,4-Dichlorophenyl)-N^4,N^4,N^6,N^6-tetraethyl-1,3,5-triazine-2,4,6-triamine (**3g**).* White solid, mp 112–114 °C. ^{1}H NMR (600 MHz, DMSO-d_6, δ ppm): 9.23 (1H, s, –NH–), 8.44 (1H, d, J = 3.0 Hz, H_{Ar}), 7.53 (1H, dd, J = 9.0, 3.0 Hz, H_{Ar}), 7.45 (1H, d, J = 9.0 Hz, H_{Ar}), 3.54–3.50 (8H, m, –CH_2–), 1.14–1.05 (12H, m, –CH_3). ^{13}C NMR (125 MHz, DMSO-d6, δ ppm): 163.9, 163.8, 141.2, 130.5, 130.0, 122.0, 120.1, 118.8, 40.8, 13.4. LC-MS (m/z) $[M + H]^+$ calcd for $C_{17}H_{25}N_6Cl_2$ 383.1512, found 383.1490.

*N-(2,4-Dichlorophenyl)-4,6-di(piperidin-1-yl)-1,3,5-triazin-2-amine (**4a**).* White solid, mp 144–146 °C. ^{1}H NMR (500 MHz, DMSO-d_6, δ ppm): 8.06 (1H, s, –NH–), 7.93 (1H, d, J = 7.5 Hz, H_{Ar}), 7.59 (1H, d, J = 2.0 Hz, H_{Ar}), 7.38 (1H, dd, J = 7.5, 2.0 Hz, H_{Ar}), 3.64 (8H, s, –CH_2–), 1.59 (4H, t, J = 4.0 Hz, –CH_2–), 1.47 (8H, d, J = 5.0 Hz, –CH_2–). ^{13}C NMR (125 MHz, DMSO-d_6, δ ppm): 164.3, 164.1, 135.6, 128.5, 127.2, 127.1, 126.5, 126.1, 43.5, 25.3, 24.3. LC-MS (m/z) $[M + H]^+$ calcd for $C_{19}H_{25}Cl_2N_6$ 407.1512, found 407.1506.

*N-(2,4-Dichlorophenyl)-4,6-bis(4-methylpiperidin-1-yl)-1,3,5-triazin-2-amine (**4b**).* White solid, mp 170–171 °C. ^{1}H NMR (500 MHz, DMSO-d_6, δ ppm): 8.06 (1H, s, –NH–), 7.93 (1H, d, J = 7.5 Hz, H_{Ar}), 7.59 (1H, d, J = 2.0 Hz, H_{Ar}), 7.39 (1H, dd, J = 7.5, 2.0 Hz, H_{Ar}), 4.54 (4H, d, J = 7.0 Hz, –CH_2–), 2.75 (4H, t, J = 10.5 Hz, –CH_2–), 1.63–1.58 (6H, m, –CH_2– and –CH<), 0.98 (4H, q, J = 8.0 Hz, –CH_2–), 0.90 (6H, d, J = 5.0 Hz, –CH_3). ^{13}C NMR (125 MHz, DMSO-d_6, δ ppm): 164.3, 164.1, 135.5, 128.5, 127.2, 127.1, 126.4, 126.0, 42.9, 33.6, 30.6, 21.7. LC-MS (m/z) $[M + H]^+$ calcd for $C_{21}H_{29}Cl_2N_6$ 435.1825, found 435.1825.

*N-(2,4-Dichlorophenyl)-4,6-di(pyrrolidin-1-yl)-1,3,5-triazin-2-amine (**4c**).* White solid, mp 129–130 °C. ^{1}H NMR (500 MHz, DMSO-d_6, δ ppm): 8.30 (1H, d, J = 7.5 Hz, H_{Ar}), 7.60 (1H, s, –NH–), 7.54 (1H, d, J = 2.0 Hz, H_{Ar}), 7.35 (1H, dd, J = 7.5, 2.0 Hz, H_{Ar}), 3.46 (8H, t, J = 5.5 Hz, –CH_2–), 1.87 (8H, t, J = 5.5 Hz, –CH_2–). ^{13}C NMR (125 MHz, DMSO-d_6, δ ppm): 163.1, 162.8, 135.4, 127.9, 126.9, 126.1, 124.3, 124.2, 45.3, 24.3. LC-MS (m/z) $[M + H]^+$ calcd for $C_{17}H_{21}Cl_2N_6$ 379.1199, found 379.1196.

*N-(2,4-Dichlorophenyl)-4,6-dimorpholino-1,3,5-triazin-2-amine (**4d**).* White solid, mp 204–205 °C. ^{1}H NMR (500 MHz, DMSO-d_6, δ ppm): 8.31 (1H, s, –NH–), 7.84 (1H, d, J = 7.0 Hz, H_{Ar}), 7.60 (1H, d, J = 2.0 Hz, H_{Ar}), 7.38 (1H, dd, J = 7.5, 2.0 Hz, H_{Ar}), 3.64 (8H, s, –CH_2–), 3.59 (8H, t, J = 4.0 Hz, –CH_2–). ^{13}C NMR (125 MHz, DMSO-d_6, δ ppm): 164.6, 164.1, 135.3, 128.5, 127.8, 127.3, 127.2, 126.8, 65.9, 43.2. LC-MS (m/z) $[M + H]^+$ calcd for $C_{17}H_{21}Cl_2N_6O_2$ 411.1098, found 411.1096 $[M - H]^-$ calcd for $C_{17}H_{18}Cl_2N_6O_2$ 409.0952, found 409.0947.

*N-(2,4-Dichlorophenyl)-4,6-bis(4-methylpiperazin-1-yl)-1,3,5-triazin-2-amine (**4e**).* White solid, mp 173–175 °C. ^{1}H NMR (500 MHz, DMSO-d_6, δ ppm): 8.27 (1H, s, –NH–), 7.88 (1H, d, J = 7.0 Hz, H_{Ar}), 7.61 (1H, d, J = 2.0 Hz, H_{Ar}), 7.41 (1H, d, J = 7.5, 2.0 Hz, H_{Ar}), 3.67 (8H, s, –CH_2–), 2.30 (8H, s, –CH_2–), 2.19 (6H, s, –CH_3). ^{13}C NMR (125 MHz, DMSO-d_6, δ ppm): 164.4, 163.9, 135.1, 128.2, 127.2, 126.9, 126.4, 125.7, 54.1, 45.4, 42.5. LC-MS (m/z) $[M + H]^+$ calcd for $C_{19}H_{27}Cl_2N_8$ 437.1730, found 437.1716.

*N-(2,4-Dichlorophenyl)-4,6-di(piperazin-1-yl)-1,3,5-triazin-2-amine (**4f**).* White solid, mp 246–248 °C. ^{1}H NMR (500 MHz, DMSO-d_6, δ ppm): 8.00 (1H, d, J = 7.5 Hz, H_{Ar}), 7.94 (1H, s, –NH–), 7.56 (1H, d, J = 2.0 Hz, H_{Ar}), 7.39 (1H, dd, J = 7.5, 2.0 Hz, H_{Ar}), 3.75–3.70 (4H, m, –CH_2–), 3.63–3.59 (4H, m, –CH_2–), 2.74–2.68 (4H, m, –CH_2–), 2.51–2.49 (4H, m, –CH_2–). ^{13}C NMR (125 MHz, DMSO-d_6, δ ppm): 164.4, 163.9, 135.2, 128.2, 127.1, 126.9, 126.0, 125.6, 44.0, 42.3. LC-MS (m/z) $[M + H]^+$ calcd for $C_{17}H_{23}Cl_2N_8$ 409.1417, found 409.1429.

4.3. *In vitro* anticancer activity

The cytotoxic potential of chlorophenylamino-*s*-triazine derivatives was assessed against two cancer cell lines (MCF7 – ATCC HTB-22 and C26 – ATCC CRL-2638) using the methyl thiazolyl tetrazolium (MTT) assay, performed in accordance with established protocols. paclitaxel (PTX) served as the positive control. Firstly, cell lines were seeded into 96-well plates at a density of 5000 cells per well and cultured at 37 °C in a 5% CO_2 atmosphere for 24 h in a growth medium supplemented with 2 mM L-glutamine, 100 IU mL^{-1} penicillin, 100 μg mL^{-1} streptomycin, Eagle's Minimum Essential Medium, and 10% fetal calf serum. Subsequently, serial dilutions of the test compounds and reference drug (PTX) in DMSO were added to the wells, followed by a 24 h incubation. A 10 μL aliquot of fresh MTT reagent was added to each well, and the plates were incubated at 37 °C in a CO_2 incubator for 4 h until a purple formazan precipitate formed.[23] The cells were subsequently lysed in ethanol, and the optical density was measured at 570 nm. The percentage of cell proliferation inhibition was calculated using the formula:

$$\text{Viability cells inhibition (\%)} = 100 - \left[\frac{(A_t - A_b)}{(A_c - A_b)}\right] \times 100\%$$

where A_t is the absorbance of the test compound-treated cells, A_b is the absorbance of the blank (medium only), and A_c is the absorbance of the untreated control cells.

The IC_{50} values, representing the compound concentration required to inhibit 50% of cell proliferation, were determined by plotting the inhibition percentages against the logarithm of the compound concentrations and fitting the data to a dose–response curve using GraphPad Prism 10.

4.4. ADME-Tox predictions

The physicochemical properties and *in silico* ADMET (absorption, distribution, metabolism, excretion, and toxicity) profiles of the compounds were evaluated using the ADMETlab 3.0 descriptor algorithm, adhering to established computational protocols.[23,40]

4.5. Molecular docking

Molecular structures of the ligands and reference drugs were constructed using ChemBioDraw 19.0, followed by energy

minimization in ChemBio3D 19.0 to optimize their conformational stability. These energy-minimized ligands were then employed as input for molecular docking simulations performed with AutoDock Vina. Anticancer protein targets, including EGFR, VEGFR2, and PI3K, were obtained from the Protein Data Bank (Table 5). For each target, water molecules were removed, and polar hydrogens along with Kollman charges were added to prepare the protein structures. AutoDock Tools was utilized to define the grid box parameters for the docking simulations. The docking protocol was validated by extracting the co-crystallized ligand and re-docking it into the active site to ensure accuracy. Subsequently, the synthesized compounds and reference drugs were docked against the selected targets to determine key binding parameters using a grid-based ligand docking approach (Table 6). The interactions, including bond types, bond lengths, and interacting amino acid residues, were analyzed, and visual representations of ligand–target interactions were generated using Discovery Studio 2021 software.[23]

4.6. Statistical analysis

All data are presented as mean ± standard deviation (SD). Statistical analysis of the IC_{50} values, comparing the test compounds and reference drugs, was conducted using one-way analysis of variance (ANOVA) followed by Tukey's Honestly Significant Difference (Tukey HSD) post hoc test, performed in SPSS 26 software. Statistical significance was established at a threshold of $p < 0.05$. Graphical representations of the results were created using microsoft excel.

Author contributions

Em Canh Pham: conceptualization, methodology, investigation, data curation, supervision, writing – original draft preparation, writing – review & editing. Song-Thuong Nguyen: investigation. Kim Anh Thi Le: investigation. Tuoi Thi Hong Do: investigation, supervision. Tuyen Ngoc Truong: data curation, supervision, writing – original draft preparation, writing – review & editing.

Conflicts of interest

The authors declare that they have no known competing financial interests or personal relationships that could have appeared to influence the work reported in this paper.

Data availability

The data supporting this article have been included as part of the supplementary information (SI). Supplementary information: ADMET and docking information, and NMR spectra. See DOI: **https://doi.org/10.1039/d5ra05705a**.

Acknowledgements

This research was funded by the University of Medicine and Pharmacy at Ho Chi Minh City under contract number 07/2024/HĐ-ĐHYD, dated 29/3/2024.

References

1 K. E. Anwer, S. S. A. El-Hddad, N. E. A. Abd El-Sattar, A. El-Morsy, F. Khedr, S. Mohamady, D. E. Keshek, S. A. Salama, K. El-Adl and N. S. Hanafy, *RSC Adv.*, 2023, **13**, 35321–35338.
2 A. Mermer, İ. E. Orhan, G. Ye, N. A. Kumar and R. Danac, *Front Chem.*, 2025, **13**, 1599140.
3 P. C. Em, L. T. Tuong Vi, L. H. Huong Ha, V. T. Bich Ngoc, B. V. Long, V. T. Thao, D. V. Duy, T. N. Ngoc Vi, N. L. Bao Khanh and N. T. Tuyen, *RSC Adv.*, 2023, **13**, 399–420.
4 P. C. Em and N. T. Tuyen, *ACS Omega*, 2022, **7**, 33614–33628.
5 P. C. Em, L. T. Tuong Vi and N. T. Tuyen, *RSC Adv.*, 2022, **12**, 21621–21646.
6 P. C. Em, L. T. Tuong Vi, T. P. Long, T. N. Huong-Giang, N. L. Bao Khanh and N. T. Tuyen, *Arab. J. Chem.*, 2022, **15**, 103682.
7 P. C. Em, N. T. Tuyen, D. Hanh Nguyen, D. V. Duy and D. T. Hong Tuoi, *Med. Chem.*, 2022, **18**, 558–573.
8 B. Viira, A. Selyutina, A. T. García-Sosa, M. Karonen, J. Sinkkonen, A. Merits and U. Maran, *Bioorg. Med. Chem.*, 2016, **24**, 2519–2529.
9 R. Kumar, A. D. Singh, J. Singh, H. Singh, R. K. Roy and A. Chaudhary, *Mini Rev. Med. Chem.*, 2014, **14**, 72–83.
10 H. R. Bhat, A. Masih, A. Shakya and S. Kumar, *J. Heterocycl. Chem.*, 2020, **57**, 390–399.
11 P. Asadi, M. Alvani, V. Hajhashemi, M. Rostami and G. Khodarahmi, *J. Mol. Struct.*, 2021, **1243**, 130760.
12 L. Marín-Ocampo, L. A. Veloza, R. Abonia and J. C. Sepúlveda-Arias, *Eur. J. Med. Chem.*, 2019, **162**, 435–447.
13 A. Shakya and J. Heterocyclic, *Chem*, 2020, **57**, 2389–2399.
14 N. Adhikari, A. Kashyap, A. Shakya, S. K. Ghosh, D. R. Bhattacharyya, H. R. Bhat and U. P. Singh, *J. Heterocycl. Chem.*, 2020, **57**, 2389–2399.
15 J. Hu, Y. Zhang, N. Tang, Y. Lu, P. Guo and Z. Huang, *Bioorg. Med. Chem.*, 2021, **32**, 115997.
16 Y. Mehmood, F. Anwar, U. Saleem, S. Hira, B. Ahmad, M. Bashir, M. T. Imtiaz, S. Najm and T. Ismail, *Life Sci.*, 2021, **285**, 119994.
17 M. Tayyab Imtiaz, F. Anwar, U. Saleem, B. Ahmad, S. Hira, Y. Mehmood, M. Bashir, S. Najam and T. Ismail, *Front. Pharmacol*, 2021, **12**, 686614.
18 I. Shawish, M. S. Nafie, A. Barakat, A. Aldalbahi, H. H. Al-Rasheed, M. Ali, W. Alshaer, M. Al Zoubi, S. Al Ayoubi, B. G. De la Torre, F. Albericio and A. El-Faham, Pyrazolyl-s-triazine with indole motif as a novel of epidermal growth factor receptor/cyclin-dependent kinase 2 dual inhibitors, *Front Chem.*, 2022, **10**, 1078163, DOI: **10.3389/fchem.2022.1078163**.
19 S. Oggu, P. Akshinthala, N. K. Katari, L. K. Nagarapu, S. Malempati, R. Gundla and S. B. Jonnalagadda, *Heliyon*, 2023, **9**, e15935.
20 J. Li, L. Li, Y. Liu, J. Zhang, C. Shi, S. Zhou and H. Qiu, *Heterocycl. Commun.*, 2023, **29**, 20220152.
21 M. A. Alelaimat, M. A. Al-Sha'er and H. A. Basheer, *ACS Omega*, 2023, **8**, 14247–14263.

22 R. Dona, R. A. Rizki, N. Frimayanti and R. Hendra, *Pharm. Educ.*, 2024, **24**, 172–178.
23 P. C. Em, L. T. Bich Ngoc, N. Minh Anh, B. V. Long and N. T. Tuyen, *RSC Adv.*, 2025, **15**, 9968–9984.
24 M. I. Ali and M. M. Naseer, *RSC Adv.*, 2023, **13**, 30462–30490.
25 D. Maliszewski and D. Drozdowska, *Pharmaceuticals*, 2022, **15**, 221.
26 D. Bareth, S. Jain, J. Kumawat, D. Kishore, J. Dwivedi and S. Z. Hashmi, *Bioorg. Chem.*, 2024, **143**, 106971.
27 D. R. Shah, R. P. Modh and K. H. Chikhalia, *Future Med. Chem.*, 2014, **6**, 463–477.
28 P. Singla, V. Luxami and K. Paul, *Eur. J. Med. Chem.*, 2015, **102**, 39–57.
29 M. Henary, C. Kananda, L. Rotolo, B. Savino, E. A. Owens and G. Cravotto, *RSC Adv.*, 2020, **10**, 14170–14197.
30 T. M. Kadayat, S. Park, K. Y. Jun, T. B. Magar, G. Bist, A. Shrestha, Y. Na, Y. Kwon and E. S. Lee, *Bioorg. Med. Chem. Lett.*, 2016, **26**, 1726–1731.
31 L. Li, P. Zhao, J. Hu, J. Liu, Y. Liu, Z. Wang, Y. Xia, Y. Dai and L. Chen, *Eur. J. Med. Chem.*, 2015, **93**, 300–307.
32 A. Singh, K. Singh, K. Kaur, A. Singh, A. Sharma, K. Kaur, J. Kaur, G. Kaur, U. Kaur, H. Kaur, P. Singh and P. M. S. Bedi, *Biomedicines*, 2024, **12**, 1192.
33 M. A. Alelaimat, M. A. Al-Sha'er and H. A. Basheer, *ACS Omega*, 2023, **8**, 14247–14263.
34 I. Shawish, A. Barakat, A. Aldalbahi, W. Alshaer, F. Daoud, D. A. Alqudah, M. Al Zoubi, M. M. Hatmal, M. S. Nafie, M. Haukka, A. Sharma, B. G. de la Torre, F. Albericio and A. El-Faham, *Pharmaceutics*, 2022, **14**, 1558.
35 M. S. Raghu, C. B. P. Kumar, M. K. Prashanth, K. Y. Kumar, B. S. Prathibha, G. Kanthimathi, S. A. Alissa, H. A. Alghulikah and S. M. Osman, *New J. Chem.*, 2021, **45**, 13909–13924.
36 W. Yan, Y. Zhao and J. He, *Mol. Med. Rep.*, 2018, **18**, 4175–4185.
37 P. Pathak, P. K. Shukla, V. Kumar, A. Kumar and A. Verma, *Inflammopharmacology*, 2018, **26**, 1441–1453.
38 K. M. Al-Zaydi, H. H. Khalil, A. El-Faham and S. N. Khattab, *Chem. Cent. J.*, 2017, **11**, 39.
39 I. Shawish, A. Barakat, A. Aldalbahi, A. M. Malebari, M. S. Nafie, A. A. Bekhit, A. Albohy, A. Khan, Z. Ul-Haq, M. Haukka, B. G. de la Torre, F. Albericio and A. El-Faham, *ACS Omega*, 2022, **7**, 24858–24870.
40 L. Fu, S. Shi, J. Yi, N. Wang, Y. He, Z. Wu, J. Peng, Y. Deng, W. Wang, C. Wu, A. Lyu, X. Zeng, W. Zhao, T. Hou and D. Cao, *Nucleic Acids Res.*, 2024, **52**, W422–W431.